NACA RM E53F10

NACA

RESEARCH MEMORANDUM

ALTITUDE EVALUATION OF SEVERAL AFTERBURNER DESIGN VARIABLES ON A J47-GE-17 TURBOJET ENGINE

By Willis M. Braithwaite, Curtis L. Walker
and Joseph N. Sivo

Lewis Flight Propulsion Laboratory
Cleveland, Ohio

NATIONAL ADVISORY COMMITTEE
FOR AERONAUTICS
WASHINGTON

October 23, 1953
Declassified September 1, 1959

ERRATA NO. 1

NACA RM E53F10

ALTITUDE EVALUATION OF SEVERAL AFTERBURNER DESIGN VARIABLES ON A J47-GE-17 TURBOJET ENGINE

By Willis M. Braithwaite, Curtis L. Walker and Joseph N. Sivo

OCTOBER 23, 1953

Table II, page 24: The column of augmented jet thrust ratio $F_j F_j'$ for configuration F at an altitude of 30,000 feet should read as follows:

1.370
1.365
1.327
1.305
1.234
1.157

NATIONAL ADVISORY COMMITTEE FOR AERONAUTICS

RESEARCH MEMORANDUM

ALTITUDE EVALUATION OF SEVERAL AFTERBURNER DESIGN VARIABLES ON A J47-GE-17 TURBOJET ENGINE

By Willis M. Braithwaite, Curtis L. Walker, and Joseph N. Sivo

SUMMARY

An investigation was conducted in an NACA altitude chamber to evaluate the effectiveness of turbine-outlet gas-straightening vanes and vortex generators, fuel distribution modifications, and afterburner shell cooling as means of improving afterburner performance. Installation of the turbine-outlet gas-straightening vanes and vortex generators resulted in a lower total-pressure loss through the afterburner and an altered air-flow profile at the afterburner inlet. Therefore, it was necessary to modify the fuel distribution to provide a good fuel-air environment at the flame holder. Another result of the installation of the turbine-outlet gas-straightening vanes and vortex generators was the reduction of the afterburner shell temperature by approximately 100° R. An additional 100° R reduction in the afterburner shell temperature was obtained with a ceramic-coated corrugated liner.

The best afterburner configuration of this investigation incorporated the turbine-outlet gas-straightening vanes and vortex generators, the ceramic-coated corrugated liner, and a fuel distribution that provided a good fuel-air environment at the flame holder. This configuration had higher afterburner combustion efficiencies than the original configuration, and the altitude limit was in excess of 54,000 feet. At low altitudes, the operation of this configuration was not limited by afterburner shell temperatures.

INTRODUCTION

Current and proposed military aircraft require thrust in addition to normal engine thrust for take-off, climb, and high speed at high altitudes. Using an afterburner is one method of meeting these require-

ments for additional thrust. Accordingly, the NACA is actively conducting several related afterburner programs.

The investigation reported herein presents information on design factors and modifications of the production afterburner for the J47-GE-17 turbojet engine designed for medium temperature operation. The present report is concerned only with the afterburner performance and operating characteristics. Altitude-starting characteristics of two of the configurations in this report are discussed in reference 1. This investigation was conducted with an engine equipped with a variable-area exhaust nozzle and operated over a range of simulated flight conditions in a 10-foot-diameter altitude test chamber at the NACA Lewis laboratory.

The initial configuration was developed by the manufacturer from a previous production afterburner by incorporating design modifications indicated by investigations reported in references 2 to 5. In the present investigation, attention was focused on three primary factors in order to improve the performance and operating limits: (1) turbine-outlet gas whirl, (2) matching of the fuel distribution with the mass-flow distribution of the turbine gases, and (3) afterburner shell cooling. Previous investigations (ref. 6) indicate that turbine-outlet gas whirl can have a detrimental effect on the performance characteristics of the afterburner. Accordingly, the effect of turbine-outlet gas-straightening vanes and vortex generators on performance was evaluated in this investigation. Several fuel-spray-bar configurations were also evaluated in order to provide satisfactory matching of the fuel distribution with the mass-flow distribution. It was desirable to evaluate methods of afterburner shell cooling, since maximum thrust can be limited by afterburner shell temperatures. Two methods of cooling the afterburner shell were investigated: (1) the incorporation of a method of fuel distribution that provided a lean fuel-air mixture near the outer shell and (2) installation of a ceramic-coated corrugated liner in the burner section.

The performance with these modifications incorporated is presented over a range of altitudes up to 50,000 feet. Data are presented in tabular and graphical form to show the effects on afterburner performance of turbine-outlet gas-straightening vanes and vortex generators, fuel distribution, and a ceramic-coated corrugated liner and to illustrate the effect of variations in flight conditions on one of the best afterburner configurations.

APPARATUS AND INSTRUMENTATION

Installation

The engine was installed in an altitude chamber that is 10 feet in diameter and 60 feet long (fig. 1). A honeycomb installed in the chamber upstream of the test section straightened and smoothed the flow of the inlet air. A forward bulkhead, which incorporated a labyrinth seal around the forward end of the engine, separated the engine-inlet air from the exhaust and provided a means of maintaining a pressure difference across the engine. A 14-inch butterfly valve in the forward bulkhead provided cooling air for the engine compartment, and a rear bulkhead prevented recirculation of exhaust gases about the engine. The exhaust gas from the jet nozzle was discharged into an exhaust diffuser to recover some of the kinetic energy of the jet and thus to extend the capacity of the exhaust system. The combustion in the afterburner was observed through a periscope located directly behind the engine.

Engine

A J47-GE-17 afterburning turbojet engine was used in this investigation. The engine has a static sea-level thrust rating of 5420 pounds without afterburning at the rated engine speed of 7950 rpm and a turbine-discharge temperature of 1760° R for an inlet air temperature of 519° R. At this operating condition, the air flow is 104 pounds per second. The over-all length of the engine and afterburner is approximately 228 inches, and the maximum diameter is 41 inches. The dry weight of the engine and afterburner, including the electronic control and airframe mounted components, is 3553 pounds. The electronic control (described in ref. 1) controls the engine speed by regulating engine fuel flow and controls the turbine-outlet temperature by regulating the exhaust-nozzle area.

Afterburner Assembly

A diagram of the afterburner assembly is shown in figure 2. The following were common to all configurations: conical diffuser, two-ring V flame holder mounted by struts from the inner body, converging conical burning section, and variable-area clamshell exhaust nozzle. The conical inner body, mounted from the outer shell by four tubular rods, contained the fuel manifolds and a depressed flame seat in the downstream end. Fuel was supplied to the afterburner by an air-turbine fuel pump driven by compressor bleed air.

Modifications to the afterburner, which were incorporated in six configurations, are listed in table I. The fuel-distribution patterns and spray-bar designs are presented in figure 3. A photograph of the turbine-outlet gas-straightening vanes and vortex generators is shown in figure 4. The ceramic-coated corrugated liner is shown installed in the afterburner section in figure 5. The ceramic used was National Bureau of Standards number A418, primarily composed of chromium oxide.

The six configurations are grouped as to purposes of the modifications. The first group of modifications was selected to show the effect of straightening vanes on engine and afterburner performance. This group included the manufacturer's original configuration A and configuration B, which was made by incorporating in configuration A straightening vanes and vortex generators at the turbine outlet and a 4-inch shorter fuel mixing length (the radial fuel distribution was equivalent to that of configuration A). The shorter fuel mixing length was a result of moving the spray bars downstream of the inner-cone supporting struts to allow equidistant circumferential spacing of the bars.

The second group of configurations was selected to illustrate the effect of modified fuel distribution. These configurations were geometrically similar, all having straightening vanes, vortex generators, and corrugated liners. Configuration C had a radial fuel distribution equivalent to the original configuration A. In configurations D and E, the fuel distribution was modified to compensate for the shift in mass-flow profile caused by the installation of the straightening vanes and vortex generators. This modification was based on the total-pressure profile at the diffuser outlet. The spray bar for configuration D had equally spaced holes of varied diameters, while the bar for configuration E had varied spacing of equally sized holes. The bar for configuration E, designed by the manufacturer, was a uniorifice bar with a metering orifice at the inlet to the bar that permitted the use of larger spray holes to prevent plugging by foreign material in the fuel.

The third group of modifications was selected to evaluate several methods of cooling the outer shell. Configurations A, B, C, and F are compared. Configuration A was the original configuration already described. Configuration F had a fuel distribution that was lean near the outer shell but was otherwise the same as configuration A. Configuration B differed from configuration A in that turbine-outlet gas-straightening vanes and vortex generators were added, and configuration C differed from configuration B only by the addition of the corrugated liner.

Instrumentation

Engine-inlet air flow was determined by pressure and temperature measurements at the compressor inlet (station 1, fig. 6(a)). Instrumen-

tation measured the engine midframe air bleed, which was subtracted from the engine-inlet air flow in order to obtain the afterburner air flow. Turbine-outlet temperature was calculated from engine performance, and turbine-outlet temperature for the electronic control was determined by averaging the engine manufacturer's eight thermocouples. The angle of whirl of the gas flow was measured at the diffuser outlet by means of a rotatable rake (fig. 6(b)). Twenty-five thermocouples attached to the afterburner shell measured temperatures at station 8, located $79\frac{5}{8}$ inches downstream of the turbine-outlet flange (fig. 6(c)). Total pressures at the exhaust-nozzle inlet were obtained with a water-cooled survey rake (fig. 6(d)), and ambient pressure in the region of the exhaust-nozzle outlet was determined by static-pressure probes in the plane of the exhaust nozzle. Engine and afterburner fuel flows were measured by calibrated rotameters. The fuel used in this investigation was MIL-F-5624A grade JP-4.

PROCEDURE

The inlet and exhaust conditions for these tests were determined by the altitude and flight Mach number according to NACA standard atmosphere; 100-percent ram pressure recovery was assumed. Afterburner performance data were obtained over a range of altitudes from 15,000 to 50,000 feet at a flight Mach number of 0.6 and a range of flight Mach numbers from 0.4 to 1.0 at an altitude of 30,000 feet. For each flight condition, data were obtained at rated engine speed and turbine-outlet temperature as maintained by the electronic integral control for a range of fuel-air ratios.

The range of fuel-air ratios at each flight condition represents, in general, the practical operating range for the afterburner. The rich operating limit was determined by afterburner shell temperature limit (2010° R) or by maximum nozzle opening. It should be noted that, with the electronic control, exhaust-nozzle area is a function of exhaust-gas temperature. Therefore, maximum nozzle opening was either the physical limit of the nozzle or the area obtained with maximum temperature for those configurations that reached a point of decreasing temperature with increasing fuel flow. The lean limit of operation was indicated by unsteady (oscillatory) combustion in the afterburner or blow-out of the flame. Over the range of conditions investigated (turbine-outlet pressures up to 2950 lb/sq ft with fuel-air ratios up to 0.04), this unsteady combustion at the lean limit was the only oscillatory combustion phenomenon encountered. No significant altitude limits were obtained for these configurations because of limitations of the altitude exhaust facilities. For afterburning conditions, the facility was limited to about 54,000 feet, which corresponds to a turbine-outlet total pressure of about 580 pounds per square foot.

The jet thrust produced by the engine and afterburner was measured by a self-balancing null-type pneumatic thrust cell. A sketch of the linkage from the engine to the thrust cell is presented in figure 1(b). The symbols and methods of calculation are presented in the appendix.

RESULTS AND DISCUSSION

The results of this investigation are discussed in relation to the three factors considered for improving the afterburner performance; that is, (1) reduction of whirl in the turbine-outlet gas, (2) matching of the fuel distribution with the mass-flow distribution, and (3) cooling of the afterburner shell. The altitude performance data are presented in tabular form in table II and in graphical form in figures 7 to 17.

Effects of Turbine-Outlet Gas-Straightening Vanes and Vortex Generators on Afterburner Performance

The performance of an afterburning engine may be detrimentally affected by high angle of whirl of the turbine-outlet gases (ref. 6). The addition of a whirl velocity produces high resultant velocities that make burning more difficult. Furthermore, a high angle of whirl produces high total-pressure losses in the burner that are particularly noticeable during nonafterburning operation. Whirl losses are less pronounced during combustion, probably because the high level of turbulence during combustion reduces the whirl component of the flow.

Since whirl angle increases with diffusion (ref. 7), measurements of the whirl were made at the diffuser outlet to obtain the maximum angle and the results are presented in figure 7. The method of obtaining this curve is the same as used in reference 6. The direction of whirl was opposite to turbine rotation, as indicated by the negative angles on figure 7, and was greater than 30° over most of the passage. The installation of the turbine-outlet gas-straightening vanes and vortex generators, designed by the manufacturer to reduce the whirl angle and to provide a uniform velocity profile, resulted in only 10° whirl in the same counterrotational direction.

Effect on afterburner-inlet temperature and pressure profiles. - Installation of the turbine-outlet gas-straightening vanes and vortex generators caused a shift in afterburner-inlet temperature profile in relation to the control thermocouple. After the vanes and vortex generators were installed, the average burner-inlet gas temperature was from 40° to 70° R lower for the same indicated control temperature.

This effect can be seen by inspection of data from table II. The setting of turbine-outlet temperature with the manufacturer's instrumentation resulted in operation at a lower turbine-outlet temperature and resulting lower nonafterburning thrusts for the configurations having straightening vanes and vortex generators.

Another effect of the straightening vanes and vortex generators was a slightly more uniform total-pressure distribution (fig. 8) at the diffuser-outlet (station 6). This trend in total-pressure profile indicates more nearly uniform mass-flow and velocity distribution of the combustion gases. However, a comparison of the pressure levels on figure 8 is invalid because of the different temperature levels.

Effect on internal performance. - A comparison of the total-pressure-loss ratios before and after the straightening vanes and vortex generators were installed is presented in figure 9. In the configuration with vanes and vortex generators (configuration B), the turbine-outlet total-pressure measurements were made downstream of the vanes. Therefore, the total-pressure loss through the straightening vanes and vortex generators was not included in the pressure-loss ratio, defined as the ratio of the total-pressure loss through the burner to the burner-inlet total pressure. The pressure-loss ratio through the vanes and vortex generators was determined to be approximately 0.025 at 30,000 feet and 0.035 at 50,000 feet from the engine pumping characteristics. This value has been added to the data on figure 9 for configuration B, and the combined pressure loss is shown by the dashed curve. Thus the installation of the straightening vanes and vortex generators reduced the over-all pressure-loss ratio by 0.02 to 0.01, the greater reduction occurring at low fuel-air ratios where the whirl is believed to have been greater.

The afterburner combustion efficiencies before (configuration A) and after (configuration B) straightening vanes and vortex generators were installed are compared in figure 10(a). For the range of fuel-air ratios investigated there was no appreciable difference in combustion efficiency at 30,000 feet, while at 50,000 feet the configuration with vanes and vortex generators had lower combustion efficiency. This loss in efficiency with vanes was due to a poor fuel-air distribution. The fuel distribution was designed for the mass-flow profile that existed before the vanes were installed. Following installation of the vanes, this mass-flow profile was modified, but the fuel distribution remained the same and resulted in a different fuel-air ratio profile.

The decrease in combustion efficiency for configuration B at 50,000 feet resulted in lower exhaust-gas temperatures (fig. 10(b)). The lower turbine-outlet temperatures also contributed to the decrease in afterburner exhaust-gas temperature.

Effect on over-all performance. - As previously noted, the effect of the straightening vanes and vortex generators was to reduce the afterburner pressure loss, and an increase in thrust would be expected. However, because of the difference in turbine-outlet conditions in this investigation, the increase in thrust was not realized and the augmented jet thrust ratio was the only valid basis for thrust comparison. (The nonafterburning jet thrust was calculated for each point with the turbine-outlet conditions obtained at that point and with the pressure drop assumed through a standard tail pipe as explained in the appendix.) The augmented jet thrust ratios are presented in figure 10(c). At 30,000 feet, where combustion efficiency was essentially the same, installation of the straightening vanes and vortex generators resulted in an increased jet thrust ratio of about 0.03. At 50,000 feet, however, the reduction in combustion efficiency countered the reduction in afterburner pressure loss, and an increase of only 0.01 was observed in jet thrust ratio.

Net thrust specific fuel consumption, presented in figure 10(d), is affected by the tail-pipe pressure loss, turbine-outlet gas temperature, and combustion efficiency. At 30,000 feet, combustion efficiency was unaffected by the turbine-outlet gas-straightening vanes, and the reduced tail-pipe pressure loss should have resulted in decreased specific fuel consumption. However, the lack of improvement illustrates the fact that the control should be rescheduled to give the same engine operating conditions after the temperature profile shift due to the installation of the straightening vanes. Also, the shift in mass-flow profile due to the addition of the vanes required an alteration to the fuel distribution to prevent a decrease in combustion efficiency at 50,000 feet. The results of modifying the fuel distribution after straightening vanes and vortex generators were installed are discussed in the following section.

Effect of Fuel Distribution on Performance

The installation of the turbine-outlet straightening vanes and vortex generators resulted in a loss in combustion efficiency that was attributed to a poor fuel-air distribution. Before alteration of the fuel system, a ceramic-coated corrugated liner was installed, the effects of which will be discussed later. Configurations C, D, and E differed only in fuel distribution.

A comparison of the combustion efficiency of configuration C, which had a fuel distribution equivalent to the original configuration

A, and configuration D, which had a fuel distribution designed to match the mass-flow profile, is presented in figure 11(a). The peak efficiency of configuration D occurred at higher fuel-air ratios than it did for configuration C. Also, configuration D had about 0.11 higher combustion efficiency than configuration C at 50,000 feet. For example, at 50,000 feet, combustion efficiency for configuration D had a peak value of 0.82 at a fuel-air ratio of 0.037 and was about 0.70 at a fuel-air ratio of 0.06.

The exhaust-gas temperature (fig. 11(b)) and net thrust ratio (fig. 11(c)) were higher for configuration D above a fuel-air ratio of 0.035 at 30,000 and 40,000 feet and higher at all fuel-air ratios investigated at 50,000 feet. Net thrust specific fuel consumption (fig. 11(d)) was lower for configuration D above a fuel-air ratio of 0.035 at 30,000 and 40,000 feet and lower at all fuel-air ratios investigated at 50,000 feet. The redesigned fuel distribution provided an improvement in combustion efficiency at fuel-air ratios in excess of 0.035 and, hence, in over-all afterburner performance.

Comparison of configurations D and E (figs. 11(a) to (c)) shows that the use of equal-diameter spray holes with various spacing (configuration E) resulted in about the same performance as with various-diameter spray holes with equal spacing (configuration D). Furthermore, the use of a metering orifice at the inlet to the spray bar did not affect performance.

Afterburner Shell Cooling

A maximum temperature limit of 2010° R for the afterburner shell was imposed by the structural strength requirements of the afterburner. The shell temperature of an afterburner is a function of the exhaust-gas temperature and the burner pressure (gas density). It was found that with a rich fuel-air mixture the original configuration A was limited at 30,000 feet and below by maximum shell temperature. Therefore, to permit higher exhaust-gas temperatures at low altitudes, methods of cooling the afterburner shell were investigated.

Reduction in turbine-outlet whirl. - A reduction in the temperature of the afterburner shell of from 80° to 120° R resulted from the installation of the straightening vanes and vortex generators (fig. 12) at an exhaust-gas temperature of 3100° R and altitudes of 30,000 and 50,000 feet. The larger reduction occurred at the lower altitude, where shell cooling was more critical. The data further indicate that the reduction would have been greater at higher fuel-air ratios. This decrease in shell temperature with the installation of straightening vanes was due to two factors. The decrease in whirl reduced the

tendency for the fuel to centrifuge toward the outer shell and also probably increased the thickness of the boundary layer at the outer shell.

Fuel distribution moved away from shell. - A previous investigation (ref. 5) showed that shell temperatures could be lowered by modifying the fuel distribution to reduce the amount of burning near the shell. Configuration F incorporates such a modification, as shown by a comparison of figures 3(a) and (e). This modification reduced the shell temperature approximately 30° at 30,000 feet (fig. 12). However, it lowered the altitude limit from over 54,000 feet for configuration A to 50,000 feet for configuration F at a flight Mach number of 0.6.

Ceramic-coated corrugated liner. - Configuration C incorporated a ceramic-coated corrugated liner installed in the afterburner in addition to the straightening vanes and vortex generators. Over the range of exhaust-gas temperatures investigated, the combination of straightening vanes and liner reduced the temperature 200° to 300° R. For configuration C an increase in exhaust-gas temperature from 2800° to 3300° R at 30,000 feet (fig. 12(b)) resulted in only 50° R increase in shell temperature. The combination of straightening vanes and liner was the most effective means of reducing shell temperatures investigated and was equivalent to the use of approximately 8 percent of engine air flow for cooling air in a conventional convective cooling system.

The coating used on the liner was a Bureau of Standards number A418 ceramic. After approximately 33 hours of afterburning, the coating and liner showed no evidence of deterioration.

A comparison of the shell temperatures for the three configurations (A, B, and C) over a range of turbine-outlet pressures with an exhaust-gas temperature of 3100° R is presented in figure 13. The temperature for the original configuration A increased with increasing pressure, while that for configuration C (liner plus straightening vanes and vortex generators) was essentially constant. This figure illustrates the greater effectiveness of the vanes and liner at low altitudes (high burner pressures), where shell temperatures were found to be critical on the original configuration.

Performance of Final Configuration

Performance data are presented for configuration D over a range of altitudes from 15,000 to 50,000 feet at a flight Mach number of 0.6, and for flight Mach numbers of 0.4 and 0.8 at an altitude of 30,000

feet. This configuration was used for evaluation because it had performance and operating and cooling characteristics equivalent or superior to any of the other configurations.

Effect of altitude and flight Mach number variations. - For a given afterburner fuel-air ratio, increasing the altitude at a constant flight Mach number tended to lower the combustion efficiency, exhaust-gas temperature, and augmented net thrust ratio (fig. 14). The peak combustion efficiency decreased from 96 percent for an afterburner fuel-air ratio of 0.027 at 15,000 feet to 82 percent for a fuel-air ratio of 0.037 at 50,000 feet. The corresponding exhaust-gas temperatures were 2960° and 2880° R. For a constant fuel-air ratio of 0.03, the temperature decreased from 2960° R at 15,000 feet to 2710° R at 50,000 feet, while the combustion efficiency decreased from 96 to 76 percent. For a wide-open exhaust nozzle, the exhaust-gas temperature decreased from 3550° R at 30,000 feet at a fuel-air ratio of 0.056 (high temperature data were not obtained at 15,000 ft) to 3380° R at 50,000 feet at a fuel-air ratio of 0.061. This decrease resulted in a decrease in augmented net thrust ratio from 1.6 to 1.52.

The net thrust specific fuel consumption decreased as the altitude increased up to an altitude between 30,000 and 40,000 feet. A further increase in altitude resulted in an increase in specific fuel consumption. This decrease was due to the increasing engine cycle efficiency with the decreasing compressor-inlet temperature as the altitude increased until the tropopause (35,000 ft) was reached, which more than compensated for the decrease in combustion efficiency. Above the tropopause, the temperature remained constant, and the decreasing combustion efficiency caused an increase in specific fuel consumption.

The effect of varying flight Mach number at an altitude of 30,000 feet is presented in figure 15. A decrease in flight Mach number affected the afterburner combustion efficiency (fig. 15(a)) and the exhaust-gas temperature (fig. 15(b)) in the same manner as did an increase in altitude; that is, combustion efficiency and exhaust-gas temperature decreased with decreasing Mach number for a given afterburner fuel-air ratio. However, since the range of flight Mach numbers was small (0.8 to 0.4), the effect was slight. The augmented net thrust ratio (fig. 15(c)) decreased with decreasing Mach number, but the net thrust specific fuel consumption (fig. 15(d)) increased as a result of the decreasing combustion efficiency.

Afterburner combustion efficiency as a function of turbine-outlet total pressure is presented in figure 16 for afterburner fuel-air ratios of 0.025, 0.035, 0.045, and 0.055. At the low fuel-air ratio, the efficiency decreased rapidly with decreasing pressure, but decreasing pressure affected the efficiency less at the higher fuel-air ratios.

Thrust Generalization

A method of generalizing jet thrust for a turbojet engine has been developed in reference 8. The basis of this method is that the jet thrust is a function of the flow through a nozzle and may, therefore, be described in terms of the nozzle-inlet total pressure, the ambient static pressure, and the throat area of the nozzle. If the experimentally determined jet thrust is adjusted for nozzle area variation, it will generalize when plotted against $(1.25P_9 - p_0)$. This method of generalization provides a calibration that may be used in determining turbojet engine jet thrust in a flight installation for take-off and flight conditions.

This method of generalizing jet thrust has been used for the data of configuration D (fig. 17). The factor used to adjust the jet thrust for area variations of the variable-area nozzle, which is presented in figure 17(b), is the ratio of jet thrust to jet thrust for maximum nozzle area as a function of the ratio of actual nozzle area to maximum nozzle area. Therefore, the jet thrust presented in figure 17(a) is the jet thrust obtainable with the maximum nozzle area.

The generalized thrust curve may be used to obtain the jet thrust for a given flight condition and afterburner fuel-air ratio. The values of the exhaust-nozzle-inlet total pressure and ambient static pressure may be obtained from the flight conditions and the engine characteristics. With these data, the jet thrust for maximum nozzle area can be obtained. The exhaust-nozzle area for a given afterburner fuel-air ratio can be obtained from figure 17(c), and from this the ratio of jet thrust at the given exhaust-nozzle area to the jet thrust at maximum nozzle area can be obtained. A numerical example of this calculation is given in the appendix.

CONCLUDING REMARKS

An investigation of the J47-GE-17 afterburning engine showed that the installation of turbine-outlet gas-straightening vanes and vortex generators reduced the counterrotational whirl by approximately 20°. This change modified the burner-inlet (turbine-outlet) total-temperature profile so that the calculated average turbine-outlet gas temperature was from 40° to 70° R lower for the same indicated control temperature. This decrease in turbine-outlet temperature resulted in lower thrust for the same afterburner fuel-air ratio. However, the total-pressure-loss ratio was reduced by 0.01 to 0.02, and the augmented jet thrust ratio was increased by 0.01 to 0.03. Because of a change in total-pressure profile and thus a change in mass-flow profile with the same fuel distribution, the fuel-air distribution

at the flame holder was not as suitable with the vanes and vortex generators, and the combustion efficiency decreased.

By adjusting the fuel distribution to the mass-flow profile that resulted from the installation of the straightening vanes and vortex generators, the loss in combustion efficiency was overcome. The peak value at 50,000 feet altitude was approximately 82 percent at a fuel-air ratio of 0.037 and was about 70 percent at a fuel-air ratio of 0.06. The combustion efficiency, the exhaust-gas temperature, and the augmented net thrust ratio were higher at higher fuel-air ratios, while net thrust specific fuel consumption was lower for the modified fuel distribution. The final fuel distribution was achieved both with spray bars having equally spaced various-diameter holes and uniorifice spray bars having variously spaced equal-diameter holes.

Afterburner shell temperatures were reduced approximately 100° R by the installation of the straightening vanes and vortex generators for an exhaust-gas temperature of 3100° R at 30,000 feet altitude. An additional reduction of 100° R in shell temperature was achieved by the installation of a ceramic-coated corrugated liner. The liner was used for approximately 33 hours of afterburner operation with no noticeable deterioration or change in appearance.

Except at the lean limit of combustion, no oscillatory combustion was encountered during this investigation, which covered burner pressures up to 2950 pounds per square foot with fuel-air ratios up to 0.04.

Lewis Flight Propulsion Laboratory
National Advisory Committee for Aeronautics
Cleveland, Ohio, May 18, 1953

APPENDIX - CALCULATIONS

Symbols

The following symbols are used in this report:

A	cross-sectional area, sq ft
C_V	velocity coefficient, ratio of actual jet velocity to effective jet velocity
F_j	jet thrust, lb
F_j'	calculated nonafterburning jet thrust, lb
F_n	net thrust, lb
F_n'	calculated nonafterburning net thrust, lb
f	fuel-air ratio
g	acceleration due to gravity, 32.2 ft/sec^2
h	enthalpy, Btu/lb
h_c	lower heating value of fuel, Btu/lb
M	Mach number
P	total pressure, lb/sq ft abs
P_9'	total pressure at exhaust-nozzle survey station in standard engine tail pipe, lb/sq ft abs
p	static pressure, lb/sq ft abs
R	gas constant, 53.4 ft-lb/(lb)($^\circ$R)
T	total temperature, $^\circ$R
V	velocity, ft/sec
V_{ef}	effective velocity, ft/sec
W_a	air flow, lb/sec

$W_{a,c}$	compressor leakage air flow, lb/sec
W_f	fuel flow, lb/hr
W_f/F_n	specific fuel consumption based on total fuel flow and net thrust, (lb/hr)/lb thrust
W_g	gas flow, lb/sec
γ	ratio of specific heats for gases
η	combustion efficiency

Subscripts:

a	air
ab	afterburner
e	engine
f	fuel
g	gas
m	maximum exhaust-nozzle area
n	exhaust-nozzle outlet, vena contracta
nc	nozzle cooling
s	labyrinth seal
T	total
tc	turbine cooling
tp	turbine pump
0	free-stream conditions
1	engine inlet
3	compressor outlet at engine combustor inlet
5	turbine outlet or tail-pipe diffuser inlet

9 exhaust-nozzle inlet

10 exhaust-nozzle outlet

Methods of Calculations

Flight Mach number and airspeed. - Flight Mach number and equivalent airspeed were calculated from engine-inlet total pressure and temperature and free-stream static pressure with complete total-pressure ram recovery assumed:

$$M_0 = \sqrt{\frac{2}{\gamma_1 - 1}\left[\left(\frac{P_1}{p_0}\right)^{\frac{\gamma_1 - 1}{\gamma_1}} - 1\right]}$$

and

$$V_0 = M_0 \sqrt{\gamma_1 g R T_1 \left(\frac{p_0}{P_1}\right)^{\frac{\gamma_1 - 1}{\gamma_1}}}$$

Air flow. - Air flow was determined from pressure and temperature measurements obtained in the engine-inlet annulus by the following equation:

$$W_{a,1} = 0.98 p_1 A_1 \sqrt{\frac{2\gamma_1 g}{(\gamma_1 - 1)RT_1}\left[\left(\frac{P_1}{p_1}\right)^{\frac{\gamma_1 - 1}{\gamma_1}} - 1\right]\left(\frac{P_1}{p_1}\right)^{\frac{\gamma_1 - 1}{\gamma_1}}}$$

where the 0.98 accounts for the 0.02 leakage between measuring station and compressor inlet. Air flow at the compressor outlet (station 3) was obtained by deducting the compressor leakage, turbine and nozzle cooling-air flows, and compressor bleed air used to drive the turbine fuel pump:

$$W_{a,3} = W_{a,1} - W_{a,c} - W_{a,tc} - W_{a,nc} - W_{a,tp}$$

Gas flow. - Afterburner gas flow is

$$W_{g,9} = W_{a,3} + \frac{W_{f,e} + W_{f,ab}}{3600} + W_{a,tc}$$

Fuel-air ratio. - The engine fuel-air ratio is given by the following equation:

$$f_e = \frac{W_{f,e}}{3600\ W_{a,3}}$$

The afterburner fuel-air ratio used herein is defined as the weight flow of fuel injected into the afterburner plus the unburned engine fuel divided by the weight flow of unburned air entering the afterburner. By combining air flow, engine fuel flow, afterburner fuel flow, and engine combustion efficiency, the following equation for afterburner fuel-air ratio is obtained:

$$f_{ab} = \frac{(1 - \eta_e)W_{f,e} + W_{f,ab}}{3600(W_{a,3}+W_{a,tc}) - \frac{\eta_e W_{f,e}}{0.0675}}$$

where 0.0675 is the stoichiometric fuel-air ratio for the engine fuel.

The total fuel-air ratio for the engine and afterburner is

$$f = \frac{W_{f,e} + W_{f,ab}}{3600(W_{a,3} + W_{a,tc})}$$

Engine combustor efficiency. - Engine combustor efficiency is the ratio of the enthalpy rise through the engine divided by the product of engine fuel flow and the lower heating value of the fuel:

$$\eta_e = \frac{(h_{a,5} - h_{a,1}) + f_e\lambda_e}{f_e h_c}$$

where $\lambda = \frac{Am + B}{m + 1}$ (symbols of ref. 9).

Engine combustion efficiency was obtained from a correlation of the engine with a standard tail pipe. For this investigation T_5 was then obtained by solving the above equation for $h_{a,5}$.

Afterburner combustion efficiency. - Afterburner combustion efficiency was obtained by dividing the enthalpy rise through the afterburner by the product of the afterburner fuel flow and lower heating value of the fuel:

$$\eta_{ab} = \frac{(h_{a,10} - h_{a,1}) + f\lambda_{10} - \eta_e f_e h_c}{f h_c - \eta_e f_e h_c}$$

Augmented thrust. - The jet thrust of the combined engine and afterburner was determined from the thrust-system measurements by the equation

$$F_j = F_d + A_s(P_1 - p_0) + 0.80\left(\frac{1}{2}\frac{W_{a,1}}{0.98g}V_0\right)$$

where F_d is equal to the thrust-system scale reading adjusted for the pressure difference on the link connecting the thrust bed in the test chamber and the measuring cell outside the test chamber, and the last term $0.80\left(\frac{1}{2}\frac{W_{a,1}}{0.98g}V_0\right)$ is the difference between the pressure forces on the bellmouth and the momentum at the bellmouth outlet.

The augmented net thrust was obtained by subtracting the free-stream momentum of the inlet air from the jet thrust:

$$F_n = F_j - \frac{W_{a,1}}{0.98g}V_0$$

where the $\frac{W_{a,1}}{0.98}$ is the air flow into the bellmouth.

Nonafterburning jet thrust. - The jet thrust for the nonafterburning engine was calculated for each afterburning point with measured turbine-outlet total pressure, engine gas flow, calculated turbine-outlet total temperature, and an assumed tail-pipe pressure drop. Experimental data from the nonafterburning engine indicated that the total-pressure loss through a standard tail pipe between stations 5 and 9 was approximately 0.04 at rated engine speed, that is, $P_9 = 0.96P_5$. The nozzle velocity coefficient for the nonafterburning engine was assumed to be 0.99, while that for the afterburning engine was assumed to be 0.97. The jet thrust equation used was

$$F_j' = C_V W_{g,5}\sqrt{\frac{RT_5}{g}}\left(\frac{V_{ef}}{\sqrt{gRT}}\right)$$

where $(V_{ef}/\sqrt{gRT})$ is an effective velocity parameter derived in reference 10; and the nonburning net thrust was

$$F_n' = F_j' - \frac{W_{a,1}}{0.98g}V_0$$

Exhaust-gas total temperature. - The total temperature of the exhaust gas was calculated from the jet thrust and conditions existing at the exhaust nozzle:

$$T_{10} = \frac{1}{C_V^2} \frac{g}{R} \left[\frac{F_j}{W_{g,9}} \frac{1}{\left(\frac{V_{ef}}{\sqrt{gRT}} \right)} \right]^2$$

where $\left(\frac{V_{ef}}{\sqrt{gRT}} \right)$ is the effective velocity parameter.

Calculated jet thrust from generalized jet thrust. - It has been shown (ref. 8) that the jet thrust of a turbojet engine may be related to the nozzle-inlet total pressure, ambient static pressure, and area. This relation is

$$F_j \propto A_{10}(1.25P_9 - p_0)$$

This equation may be represented by two plots as figures 17(a) and (b).

For an assumed flight condition of 40,000 feet altitude and a flight Mach number of 0.6, the pressure values are found from table II as P_9 = 1009 pounds per square foot and p_0 = 392 pounds per square foot. Then

$$1.25P_9 - p_0 = 1.25(1009) - 392 = 869.5 \text{ lb/sq ft}$$

From figure 17(a), the jet thrust for an open nozzle ($A_{10,m}$ = 3.5 sq ft), which would require an afterburner fuel-air ratio of 0.0575, is 2790 pounds.

If an afterburner fuel-air of 0.040 is desired,

$$A_{10} = 3.17 \text{ sq ft (from fig. 17(c))}$$

and

$$\frac{A_{10}}{A_{10,m}} = \frac{3.17}{3.50} = 0.906$$

With the area ratio, the thrust correction ratio may be found from figure 17(b) to be

$$F_j/F_{j,m} = 0.912$$

Therefore, the jet thrust for this fuel-air ratio is

$$F_j = F_{j,m} (F_j/F_{j,m}) = 2790(0.912) = 2544 \text{ lb}$$

REFERENCES

1. Jansen, Emmert T., and Harvey, Ray W., Sr.: Transient Data Obtained During Altitude Starts of the J47-GE-17 Afterburner. NACA RM E52J17, 1952.

2. Johnson, LaVern A., and Meyer, Carl L.: Altitude Performance Characteristics of Turbojet-Engine Tail-Pipe Burner with Variable-Area Exhaust Nozzle Using Several Fuel Systems and Flame Holders. NACA RM E50F28, 1950.

3. Jansen, Emmert T., and Thorman, H. Carl: Altitude Performance Characteristics of Tail-Pipe Burner with Variable-Area Exhaust Nozzle. NACA RM E50E29, 1950.

4. Fleming, W. A., Conrad, E. William, and Young, A. W.: Experimental Investigation of Tail-Pipe-Burner Design Variables. NACA RM E50K22, 1951.

5. Conrad, E. William, and Jansen, Emmert T.: Effects of Internal Configuration on Afterburner Shell Temperatures. NACA RM E51I07, 1952.

6. Braithwaite, Willis M., Renas, Paul E., and Jansen, Emmert T.: Altitude Investigation of Three Flame-Holder and Fuel-Systems Configurations in a Short Converging Afterburner on a Turbojet Engine. NACA RM E52G29, 1952.

7. Schwartz, Ira R.: Investigations of an Annular Diffuser-Fan Combination Handling Rotating Flow. NACA RM L9B28, 1949.

8. Hesse, W. J.: A Simple Gross Thrust Meter Installation Suitable For Indicating Turbojet Engine Gross Thrust in Flight. Tech. Rep. No. 2-52, Test Pilot Training Div., Naval Air Test Station, Apr. 3, 1952.

9. Turner, L. Richard, and Bogart, Donald: Constant-Pressure Combustion Charts Including Effects of Diluent Addition. NACA Rep. 937, 1949. (Supersedes NACA TN's 1086 and 1655.)

10. Turner, L. Richard, Addie, Albert N., and Zimmerman, Richard H.: Charts for the Analysis of One-Dimensional Steady Compressible Flow. NACA TN 1419, 1948.

TABLE I. - MODIFICATIONS INCORPORATED

Configuration	Number of fuel-spray bars	Orifices per spray bar	Mixing length, in.	Spray-bar location (fig. 2(a))	Fuel distribution (fig. 3)	Modifications
A	19	10	26	1	(a)	Manufacturer's original configuration
B	20	10	22	2	(b)	Fuel distribution equivalent to to configuration A; turbine-outlet gas-straightening vanes and vortex generators added
C	20	10	22	2	(b)	Ceramic-coated corrugated liner added to configuration B
D	20	18	22	2	(c)	Modified fuel distribution; other variables same as configuration C; final configuration
E	20	16	22	2	(d)	Uniorifice spray bar with distribution of configuration D; other variables same as configuration C
F	19	10	26	1	(e)	Fuel distribution away from shell; no turbine-outlet straightening vanes, vortex generators, or coated liner

TABLE II. - ALTITUDE

Altitude, ft	Flight Mach number, M_O	Free-stream static pressure, P_O, lb/sq ft abs	Engine-inlet total pressure, P_1, lb/sq ft abs	Engine-inlet total temperature, T_1, ^oR	Turbine-outlet total pressure, P_5, lb/sq ft abs	Turbine-outlet total temperature, T_5, ^oR	Manufacturer's turbine-outlet control temperature, $T_{5,m}$, ^oR	Engine-inlet air flow, $w_{a,1}$, lb/sec	Engine fuel flow, $w_{f,e}$, lb/hr	Afterburner fuel flow, $w_{f,ab}$, lb/hr	Total fuel-air ratio, f	Afterburner fuel-air ratio, f_{ab}
												Original
15,000	0.589	1210	1530	547	2978	1776	1755	72.50	4483	7040	0.0452	0.0374
	.600	1197	1526	548	2988	1783	1745	72.12	4463	5992	.0412	.0321
	.600	1198	1528	545	2981	1781	1760	72.76	4502	5387	.0386	.0286
	.591	1207	1528	550	2976	1772	1745	72.24	4425	4672	.0358	.0249
	.599	1199	1527	549	2961	1771	1750	72.08	4434	4011	.0333	.0218
30,000	0.367	638	700	425	1614	1803	1770	38.99	2690	5303	0.0583	0.0546
	.381	631	697	425	1608	1803	1770	38.98	2688	4391	.0517	.0483
	.383	633	700	425	1611	1803	1770	39.04	2688	3629	.0460	.0374
	.351	640	697	427	1590	1793	1770	38.75	2650	2980	.0413	.0309
	.383	630	697	427	1606	1798	1765	38.82	2672	2408	.0372	.0250
	.381	631	697	426	1604	1804	1770	38.91	2680	1974	.0340	.0205
30,000	0.586	632	797	441	1807	1784	1765	43.60	2963	4693	0.0499	0.0430
	.575	640	801	441	1803	1779	1760	43.76	2954	4311	.0472	.0392
	.578	635	796	441	1798	1785	1760	43.51	2954	3821	.0443	.0351
	.585	636	800	433	1823	1778	1760	44.00	2993	3380	.0412	.0308
	.594	628	796	440	1795	1784	1765	43.55	2954	2888	.0381	.0266
	.584	633	797	441	1799	1779	1760	43.38	2937	2330	.0345	.0215
30,000	0.813	630	972	471	2124	1766	1760	51.15	3315	5655	0.0498	0.0433
	.793	633	959	468	2074	1771	1750	50.61	3297	4874	.0459	.0379
	.798	630	958	467	2082	1777	1750	50.71	3315	4112	.0416	.0319
	.792	634	959	466	2080	1769	1750	50.79	3315	3351	.0373	.0260
	.788	637	959	466	2072	1776	1745	50.57	3315	2609	.0333	.0204
	.802	630	962	466	2093	1769	1745	50.84	3320	2194	.0308	.0171
30,000	0.985	639	1188	497	2524	1789	1780	60.21	3948	4571	0.0402	0.0300
	.993	633	1189	496	2523	1775	1770	60.75	3948	4371	.0389	.0286
	.993	633	1188	497	2556	1807	1795	60.44	4013	4052	.0379	.0266
	.996	631	1188	494	2544	1779	1775	60.83	3975	3669	.0357	.0238
	.995	632	1188	494	2546	1793	1775	60.60	3985	3304	.0342	.0216
	.992	634	1188	494	2538	1786	1775	60.60	3966	2807	.0318	.0184
40,000	0.579	401	503	425	1149	1831	1780	27.77	1960	4473	0.0660	0.0653
	.581	397	499	425	1154	1831	1780	27.67	1952	3765	.0589	.0553
	.581	397	499	425	1154	1805	1775	28.10	1945	3284	.0529	.0470
	.570	398	496	425	1144	1831	1780	27.53	1945	2734	.0484	.0404
	.587	393	495	425	1150	1831	1780	27.47	1945	2312	.0441	.0343
	.570	395	493	425	1139	1844	1780	27.36	1952	1941	.0406	.0292
	.569	395	492	425	1143	1837	1780	27.38	1945	1538	.0368	.0239
50,000	0.643	239	315	436	710	1838	1770	16.97	1216	2807	0.0678	0.0679
	.628	242	316	433	710	1822	1770	17.13	1221	2610	.0619	.0622
	.643	239	316	430	711	1822	1765	17.24	1226	2261	.0578	.0538
	.630	239	312	419	724	1818	1770	17.38	1240	1901	.0516	.0457
	.609	243	312	421	720	1826	1765	17.30	1243	1672	.0482	.0401
												Configuration B, straightening
30,000	0.608	622	798	442	1727	1743	1765	43.64	2824	7040	0.0644	0.0633
	.605	623	798	441	1725	1741	1765	43.77	2824	6078	.0580	.0544
	.609	624	801	442	1730	1749	1760	43.69	2842	5240	.0527	.0472
	.605	623	797	442	1720	1743	1760	43.57	2824	4494	.0479	.0406
	.601	625	798	442	1720	1749	1760	43.62	2833	3362	.0405	.0304
40,000	0.611	385	495	423	1087	1755	1770	27.66	1840	4113	0.0614	0.0590
	.614	384	495	422	1085	1761	1765	27.72	1849	3248	.0524	.0466
	.612	385	495	421	1085	1753	1770	27.83	1849	2348	.0430	.0336
	.608	386	495	421	1094	1759	1765	27.83	1856	1816	.0376	.0261
50,000	0.642	235	310	425	665	1746	1775	17.21	1161	2229	0.0562	0.0519
	.643	235	310	424	665	1766	1775	17.19	1176	1820	.0497	.0428
	.642	235	310	425	666	1751	1775	17.24	1183	1380	.0418	.0321
	.653	235	313	424	673	1754	1775	17.29	1171	1075	.0371	.0255
												Configuration C,
15,000	0.611	1186	1525	543	2890	1778	1770	72.65	4492	8200	0.0499	0.0438
	.608	1186	1522	544	2888	1760	1765	72.71	4425	7370	.0462	.0390
	.610	1188	1526	544	2898	1753	1765	72.85	4415	6520	.0428	.0344
	.609	1186	1523	546	2897	1755	1765	72.81	4388	5695	.0395	.0301
	.610	1183	1520	546	2855	1755	1765	72.51	4369	4815	.0361	.0256
	.616	1174	1516	547	2846	1740	1755	72.09	4302	3940	.0326	.0210
	.610	1182	1519	547	2856	1744	1750	72.19	4311	3115	.0293	.0166
	.608	1184	1519	549	2872	1758	1755	71.62	4320	2645	.0277	.0143

NACA

PERFORMANCE DATA

Exhaust-nozzle-inlet total pressure, P_9, lb/sq ft abs	Exhaust-nozzle-total temperature, T_{10}, °R	Exhaust-nozzle area, A_{10}, sq ft	Afterburner temperature ratio, T_{10}/T_5	Augmented jet thrust, F_J, lb	Augmented jet thrust ratio, F_J/F'_J	Net thrust, F_n, lb	Augmented net thrust ratio, F_n/F'_n	Net thrust specific fuel consumption, $\frac{(W_{f,e}+W_{f,ab})}{F_n}$	Engine combustion efficiency, η_e	Afterburner combustion efficiency, η_{ab}	Maximum-afterburner shell temperature, °R	Afterburner pressure-loss ratio, $\frac{P_5-P_9}{P_5}$
Configuration A												
2670	3131	3.04	1.763	6248	1.297	4778	1.427	2.412	0.990	0.883	1990	0.1034
2684	3000	2.92	1.683	6106	1.262	4617	1.379	2.264	.990	.916	1910	.1018
2679	2880	2.89	1.617	6013	1.235	4514	1.339	2.191	.990	.919	1871	.1013
2688	2735	2.82	1.543	5787	1.206	4314	1.297	2.109	.990	.907	1800	.0968
2677	2574	2.72	1.453	5591	1.167	4104	1.242	2.058	.990	.866	1735	.0959
1427	3362	3.22	1.865	3552	1.341	3110	1.409	2.570	0.990	0.765	2022	0.1159
1428	3274	3.10	1.816	3500	1.317	3041	1.384	2.328	.990	.847	1931	.1120
1435	3136	2.98	1.739	3417	1.284	2955	1.344	2.138	.990	.912	1805	.1093
1419	2982	2.92	1.663	3249	1.248	2826	1.296	1.992	.990	.961	1729	.1076
1444	2670	2.79	1.485	3123	1.181	2663	1.219	1.908	.990	.857	1682	.1009
1443	2538	2.69	1.407	3037	1.144	2578	1.174	1.805	.990	.874	1549	.1004
1610	3237	3.07	1.814	4130	1.326	3341	1.436	2.292	0.990	0.874	1934	0.1090
1606	3162	3.01	1.777	4057	1.307	3278	1.410	2.216	.990	.889	1830	.1093
1609	3030	2.99	1.697	3948	1.276	3189	1.369	2.138	.990	.885	1792	.1057
1635	2899	2.92	1.630	3918	1.248	3132	1.331	2.035	.990	.896	1800	.1031
1613	2761	2.82	1.548	3772	1.213	2974	1.287	1.964	.990	.897	1750	.1014
1622	2544	2.69	1.430	3587	1.163	2804	1.219	1.878	.990	.847	1663	.0984
1894	3245	3.10	1.837	5187	1.345	3896	1.519	2.302	0.990	0.862	2101	0.1083
1856	3089	3.01	1.744	4935	1.305	3690	1.454	2.214	.990	.868	1892	.1051
1870	2923	2.95	1.645	4801	1.260	3557	1.391	2.088	.990	.884	1770	.1018
1873	2701	2.82	1.527	4601	1.212	3354	1.316	1.987	.990	.862	1714	.0995
1872	2490	2.69	1.402	4370	1.156	3134	1.232	1.890	.990	.831	1585	.0961
1900	2368	2.58	1.339	4311	1.130	3050	1.194	1.808	.990	.822	1540	.0922
2277	2758	2.82	1.653	6097	1.273	4254	1.444	2.003	0.990	0.946	1926	0.0979
2273	2863	2.79	1.613	6050	1.255	4179	1.417	1.991	.990	.921	1888	.0991
2316	2837	2.75	1.570	6018	1.239	4155	1.387	1.941	.990	.938	1897	.0939
2302	2706	2.69	1.521	5889	1.215	4016	1.351	1.903	.990	.920	1817	.0951
2307	2639	2.65	1.472	5791	1.195	3927	1.316	1.856	.990	.926	1736	.0939
2306	2460	2.56	1.377	5569	1.153	3709	1.250	1.826	.990	.854	1720	.0914
1001	3472	3.35	1.896	2738	1.363	2249	1.480	2.860	0.987	0.699	1995	0.1288
1014	3306	3.22	1.806	2669	1.327	2180	1.431	2.622	.987	.725	1910	.1213
1019	3163	3.10	1.752	2644	1.302	2148	1.393	2.434	.987	.760	1870	.1170
1017	3101	3.04	1.694	2545	1.275	2068	1.361	2.263	.987	.820	1792	.1110
1018	3018	2.95	1.648	2519	1.252	2021	1.333	2.106	.987	.887	1745	.1148
1015	2861	2.85	1.552	2408	1.211	1934	1.277	2.013	.987	.887	1678	.1089
1021	2600	2.72	1.415	2298	1.154	1824	1.202	1.910	.987	.800	1598	.1067
612	3496	3.35	1.902	1697	1.364	1364	1.497	2.949	0.967	0.684	1817	0.1377
612	3411	3.31	1.872	1680	1.347	1352	1.471	2.834	.967	.727	1820	.1381
615	3383	3.22	1.857	1684	1.338	1348	1.460	2.585	.968	.780	1781	.1351
632	3144	3.10	1.729	1644	1.287	1316	1.387	2.387	.968	.776	1717	.1270
631	3104	3.04	1.700	1607	1.271	1289	1.363	2.261	.968	.829	1668	.1244
vanes and vortex generators added												
1593	3360	3.28	1.928	4275	1.411	3456	1.563	2.854	0.990	0.679	1769	0.0776
1601	3270	3.18	1.878	4203	1.385	3386	1.527	2.629	.990	.728	1719	.0719
1611	3220	3.12	1.841	4152	1.366	3330	1.503	2.427	.990	.795	1718	.0688
1606	3152	3.08	1.808	4073	1.348	3259	1.477	2.245	.990	.866	1702	.0663
1616	2880	2.95	1.647	3867	1.279	3056	1.381	2.027	.990	.904	1659	.0605
1002	3210	3.25	1.829	2656	1.368	2146	1.500	2.774	0.987	0.654	1681	0.0782
1005	3200	3.17	1.817	2638	1.354	2125	1.481	2.399	.987	.796	1680	.0737
1013	2968	3.03	1.693	2530	1.297	2017	1.403	2.081	.987	.894	1659	.0664
1026	2669	2.87	1.517	2395	1.223	1885	1.301	1.948	.986	.848	1629	.0622
607	3108	3.24	1.780	1611	1.336	1278	1.464	2.653	0.964	0.681	1600	0.0868
611	2988	3.12	1.692	1572	1.297	1239	1.410	2.418	.966	.730	1600	.0804
615	2613	2.97	1.492	1486	1.211	1152	1.290	2.225	.963	.665	1574	.0754
627	2571	2.82	1.466	1460	1.197	1120	1.273	2.005	.966	.776	1535	.0692
straightening vanes and liner												
2691	3228	3.12	1.816	6454	1.350	4936	1.512	2.571	0.990	0.825	1561	0.0689
2695	3106	3.06	1.765	6324	1.327	4810	1.480	2.452	.990	.843	1553	.0668
2711	3008	2.97	1.716	6226	1.306	4705	1.449	2.324	.990	.873	1550	.0645
2717	2867	2.91	1.634	6063	1.271	4541	1.399	2.220	.990	.876	1540	.0621
2674	2735	2.82	1.558	5831	1.236	4313	1.348	2.129	.990	.898	1519	.0634
2677	2570	2.70	1.474	5626	1.200	4102	1.296	2.009	.990	.902	1516	.0594
2699	2322	2.58	1.331	5338	1.138	3826	1.204	1.941	.990	.790	1494	.0550
2722	2153	2.49	1.225	5107	1.091	3609	1.133	1.930	.990	.633	1490	.0522

TABLE II. - Concluded.

Altitude, ft	Flight Mach number, M_O	Free-stream static pressure, P_O, lb/sq ft abs	Engine-inlet total pressure, P_1, lb/sq ft abs	Engine-inlet total temperature, T_1, °R	Turbine-outlet total pressure, P_5, lb/sq ft abs	Turbine-outlet total temperature, T_5, °R	Manufacturer's turbine-outlet control temperature, $T_{5,m}$, °R	Engine-inlet air flow, $w_{a,1}$, lb/sec	Engine fuel flow, $w_{f,e}$, lb/hr	Afterburner fuel flow, $w_{f,ab}$, lb/hr	Total fuel-air ratio, f	Afterburner fuel-air ratio, f_{ab}
												Configuration C,
30,000	0.604	625	799	444	1723	1751	1765	43.62	2833	7773	0.0693	0.0699
	.606	621	795	443	1711	1750	1765	43.49	2833	6427	.0607	.0582
	.604	624	798	442	1721	1749	1765	43.69	2833	5137	.0520	.0463
	.609	624	802	441	1721	1742	1765	43.81	2833	3957	.0442	.0355
	.611	620	798	439	1724	1746	1765	43.73	2850	2879	.0373	.0260
	.616	622	802	445	1703	1739	1765	43.74	2807	1797	.0300	.0163
40,000	0.600	388	494	422	1093	1768	1765	27.79	1865	4431	0.0644	0.0632
	.598	388	494	422	1094	1768	1765	27.77	1865	3784	.0580	.0543
	.597	390	497	426	1091	1766	1770	27.61	1849	3005	.0500	.0433
	.608	387	496	429	1084	1767	1765	27.50	1832	2313	.0430	.0336
	.619	384	497	424	1093	1770	1765	27.71	1857	1607	.0356	.0233
	.612	387	498	421	1104	1767	1765	27.97	1872	1068	.0300	.0153
50,000	0.605	239	306	425	672	1801	1765	17.05	1197	2643	0.0644	0.0631
	.598	238	302	424	659	1792	1765	17.07	1192	2227	.0572	.0531
	.611	236	304	427	653	1758	1765	16.74	1142	1790	.0500	.0433
	.606	241	308	423	668	1806	1765	17.08	1207	1297	.0419	.0314
	.629	234	305	423	669	1806	1760	17.07	1202	669	.0313	.0167
												Configuration D, modified fuel distribution
15,000	0.614	1185	1527	539	2897	1737	1760	73.39	4387	8021	0.0482	0.0418
	.613	1189	1532	533	2947	1738	1760	74.14	4464	5800	.0395	.0301
	.614	1187	1531	537	2920	1741	1760	73.67	4434	4612	.0350	.0241
30,000	0.398	634	707	427	1546	1749	1770	39.35	2580	5614	0.0594	0.0563
	.394	532	704	426	1536	1742	1760	39.24	2562	4193	.0491	.0422
	.404	625	700	425	1528	1748	1760	39.03	2563	3033	.0409	.0308
	.412	626	704	423	1554	1740	1755	39.39	2580	1980	.0330	.0200
30,000	0.610	624	802	438	1740	1746	1765	44.18	2876	6317	0.0593	0.0563
	.608	628	805	436	1734	1738	1760	44.39	2876	5261	.0522	.0466
	.610	624	802	444	1709	1745	1755	43.65	2816	4213	.0459	.0379
	.602	625	798	445	1712	1752	1755	43.50	2833	3025	.0384	.0275
	.603	630	805	445	1723	1746	1755	43.80	2833	2028	.0334	.0207
30,000	0.809	625	961	463	2027	1754	1770	51.21	3287	7706	0.0612	0.0589
	.814	625	966	460	2031	1739	1760	51.75	3297	5906	.0507	.0446
	.804	626	959	472	1995	1749	1765	50.48	3208	4795	.0452	.0372
	.800	632	962	456	2039	1742	1760	51.66	3297	3765	.0390	.0286
	.819	620	962	455	2042	1748	1760	51.80	3324	3007	.0348	.0229
40,000	0.600	391	498	415	1104	1755	1765	28.23	1888	4094	0.0604	0.0577
	.596	393	499	416	1103	1749	1765	28.30	1880	3514	.0543	.0493
	.594	394	499	423	1095	1749	1765	28.07	1856	2844	.0477	.0402
	.600	394	502	423	1097	1755	1765	28.04	1856	2128	.0408	.0303
	.592	393	498	422	1098	1761	1770	28.00	1865	1502	.0343	.0215
50,000	0.658	235	315	420	679	1752	1775	17.55	1190	2663	0.0627	0.0609
	.636	237	311	419	678	1770	1772	17.34	1190	2505	.0609	.0583
	.619	239	310	418	678	1776	1765	17.25	1190	2194	.0560	.0515
	.653	235	312	417	672	1747	1770	17.46	1182	1874	.0499	.0433
	.638	234	308	417	672	1768	1765	17.32	1190	1513	.0446	.0356
	.637	235	309	418	668	1769	1775	17.33	1190	1229	.0398	.0290
												Configuration E, modified fuel
40,000	0.589	396	500	421	1092	1748	1750	28.07	1825	3948	0.0586	0.0553
	.610	389	500	423	1085	1742	1745	28.19	1817	3680	.0557	.0514
	.601	394	503	423	1087	1742	1745	28.15	1825	3364	.0525	.0470
	.567	403	501	423	1092	1742	1745	28.12	1825	3186	.0508	.0946
	.573	401	501	422	1091	1741	1745	28.24	1825	2778	.0465	.0387
	.584	397	500	423	1080	1742	1745	28.15	1825	2285	.0415	.0320
50,000	0.632	237	310	432	659	1793	1770	17.08	1171	2717	0.0649	0.0638
	.623	243	316	431	666	1760	1760	17.37	1151	2275	.0566	.0526
	.626	236	307	433	660	1773	1770	16.90	1142	2030	.0536	.0482
	.624	236	307	432	661	1784	1765	16.96	1157	1468	.0441	.0352
												Configuration F, original with
30,000	0.592	634	804	443	1765	1763	1760	43.67	2876	6495	0.0611	0.0587
	.590	631	798	441	1759	1774	1755	43.44	2876	5655	.0560	.0516
	.591	632	800	440	1770	1780	1760	43.67	2911	4955	.0513	.0451
	.592	628	796	445	1757	1778	1755	43.23	2868	4311	.0473	.0396
	.590	633	801	438	1774	1771	1755	43.74	2911	3228	.0400	.0294
	.590	636	804	438	1779	1778	1755	43.92	2928	2243	.0335	.0204
40,000	0.590	395	500	417	1149	1812	1780	28.07	1960	4073	0.0613	0.0587
	.593	394	500	415	1149	1810	1780	28.06	1960	3475	.0552	.0502
	.584	394	496	414	1140	1797	1770	28.01	1936	2934	.0496	.0423
	.593	391	496	426	1139	1801	1780	27.57	1896	2408	.0455	.0353
	.586	391	495	429	1130	1816	1775	27.37	1903	1901	.0396	.0282
	.590	395	500	414	1151	1803	1775	28.10	1968	1465	.0346	.0211

ALTITUDE PERFORMANCE DATA

Exhaust-nozzle-inlet total pressure, P_9, lb/sq ft abs	Exhaust-nozzle-total temperature, T_{10}, °R	Exhaust-nozzle area, A_{10}, sq ft	Afterburner temperature ratio, T_{10}/T_5	Augmented jet thrust, F_j, lb	Augmented jet thrust ratio, F_j/F'_j	Net thrust, F_n, lb	Augmented net thrust ratio, F_n/F'_n	Net thrust specific fuel consumption, $\frac{(W_{f,e}+W_{f,ab})}{F_n}$	Engine combustion efficiency, η_e	Afterburner combustion efficiency, η_{ab}	Maximum-afterburner shell temperature, °R	Afterburner pressure-loss ratio, $\frac{P_5-P_9}{P_5}$
straightening vanes and liner												
1579	3271	3.31	1.868	4209	1.390	3393	1.535	3.126	0.990	0.589	1584	0.0836
1571	3308	3.29	1.890	4185	1.388	3370	1.531	2.748	.990	.704	1599	.0818
1584	3199	3.19	1.829	4103	1.354	3288	1.484	2.424	.990	.798	1588	.0796
1597	3048	3.07	1.750	3996	1.318	3173	1.436	2.140	.990	.904	1559	.0721
1613	2783	2.89	1.594	3809	1.252	2987	1.345	1.918	.990	.955	1540	.0644
1610	2329	2.58	1.339	3446	1.143	2612	1.198	1.763	.990	.844	1489	.0546
997	3170	3.30	1.793	2654	1.353	2150	1.475	2.928	0.987	0.600	1590	0.0882
1001	3186	3.24	1.802	2637	1.349	2135	1.469	2.646	.987	.689	1592	.0850
1000	3107	3.19	1.759	2564	1.322	2064	1.434	2.352	.987	.793	1610	.0836
1000	2976	3.03	1.684	2484	1.286	1975	1.389	2.099	.986	.896	1600	.0779
1019	2652	2.82	1.498	2372	1.210	1853	1.286	1.869	.987	.920	1491	.0677
1038	2238	2.62	1.550	2193	1.108	1677	1.146	1.753	.986	.727	1460	.0598
608	3026	3.31	1.680	1573	1.301	1260	1.406	3.049	0.967	0.535	1599	0.0952
596	3022	3.26	1.686	1554	1.294	1245	1.396	2.746	.966	.617	1600	.0966
596	2925	3.15	1.664	1491	1.280	1181	1.381	2.483	.963	.687	1610	.0913
613	2686	2.96	1.487	1452	1.202	1139	1.273	2.198	.967	.707	1499	.0816
620	2129	2.65	1.179	1297	1.062	973	1.085	1.923	.967	.486	1481	.0735
with straightening vanes and liner												
2662	3408	3.19	1.962	6662	1.392	5127	1.577	2.420	0.990	0.974	1612	0.0811
2750	2957	2.95	1.701	6301	1.294	4761	1.431	2.156	.990	.954	1582	.0669
2735	2728	2.82	1.567	5986	1.241	4446	1.353	2.035	.990	.948	1569	.0634
1409	3557	3.50	2.034	3669	1.424	3185	1.522	2.572	0.990	0.841	1819	0.0886
1414	3238	3.22	1.859	3470	1.355	2991	1.437	2.259	.990	.893	1570	.0794
1421	2916	3.01	1.668	3273	1.279	2785	1.345	2.010	.990	.927	1535	.0700
1464	2365	2.69	1.359	2994	1.153	2494	1.189	1.828	.990	.741	1489	.0579
1591	3548	3.50	2.032	4415	1.434	3587	1.594	2.563	0.990	0.836	1739	0.0856
1594	3356	3.31	1.931	4274	1.391	3447	1.535	2.361	.990	.882	1587	.0807
1585	3142	3.13	1.801	4036	1.340	3212	1.467	2.188	.990	.914	1560	.0726
1602	2828	2.92	1.614	3799	1.261	2987	1.357	1.961	.990	.943	1519	.0643
1625	2456	2.72	1.407	3553	1.174	2734	1.239	1.778	.990	.808	1490	.0569
1860	3566	3.50	2.033	5474	1.447	4198	1.675	2.619	0.990	0.807	1772	0.0824
1875	3346	3.22	1.924	5312	1.395	4019	1.599	2.290	.990	.904	1590	.0768
1854	3128	3.10	1.788	4953	1.343	3689	1.522	2.169	.990	.914	1549	.0707
1910	2870	2.92	1.648	4860	1.279	3596	1.419	1.964	.990	.947	1529	.0633
1921	2614	2.75	1.495	4669	1.216	3376	1.325	1.875	.990	.901	1500	.0583
1003	3407	3.50	1.941	2773	1.400	2266	1.537	2.640	0.987	0.760	1736	0.0915
1007	3306	3.29	1.890	2722	1.375	2216	1.503	2.434	.987	.817	1590	.0870
1005	3080	3.18	1.761	2583	1.321	2078	1.433	2.262	.987	.833	1580	.0822
1015	2835	2.98	1.615	2461	1.258	1952	1.348	2.041	.987	.878	1528	.0748
1027	2393	2.75	1.359	2255	1.151	1754	1.202	1.920	.987	.709	1483	.0647
611	3384	3.46	1.932	1729	1.394	1363	1.547	2.786	0.967	0.714	1609	0.1002
612	3339	3.37	1.886	1690	1.376	1359	1.515	2.719	.967	.717	1600	.0978
614	3229	3.28	1.818	1641	1.346	1320	1.470	2.564	.967	.743	1593	.0930
613	3132	3.16	1.793	1638	1.333	1298	1.460	2.354	.965	.814	1571	.0884
618	2814	2.98	1.592	1535	1.260	1205	1.357	2.243	.967	.738	1543	.0811
618	2694	2.89	1.523	1493	1.220	1162	1.301	2.082	.967	.788	1513	.0745
distribution with uniorifice spray bar												
992	3465	3.50	1.982	2749	1.411	2250	1.553	2.566	0.985	0.815	----	0.0916
983	3308	3.22	1.899	2690	1.376	2173	1.511	2.530	.985	.791	----	.0940
988	3257	3.16	1.870	2657	1.362	2146	1.490	2.418	.985	.828	----	.0911
994	3218	3.10	1.847	2614	1.352	2130	1.469	2.353	.985	.843	----	.0898
998	3092	3.01	1.776	2568	1.322	2078	1.430	2.215	.985	.875	----	.0853
994	2907	2.89	1.669	2480	1.277	1982	1.373	2.074	.985	.901	----	.0796
596	3348	3.50	1.867	1657	1.375	1329	1.515	2.926	0.963	0.666	----	0.0956
606	3228	3.17	1.834	1622	1.355	1294	1.489	2.646	.963	.733	----	.0901
601	3146	3.06	1.774	1578	1.329	1255	1.453	2.527	.962	.743	----	.0894
607	2912	2.89	1.632	1514	1.266	1191	1.364	2.204	.961	.815	----	.0817
fuel distribution away from shell												
1564	3362	3.28	1.907	4189	1.856	3389	1.502	2.765	0.990	0.720	1912	0.1139
1561	3387	3.28	1.909	4166	1.844	3374	1.494	2.528	.990	.816	1949	.1126
1576	3231	3.16	1.815	4090	1.791	3286	1.442	2.389	.990	.829	1910	.1096
1573	3206	3.04	1.803	3976	1.765	3182	1.412	2.256	.990	.913	1790	.1047
1593	2834	2.92	1.600	3799	1.664	3004	1.316	2.044	.990	.886	1722	.1020
1608	2522	2.72	1.418	3581	1.560	2783	1.212	1.858	.990	.878	1600	.0961
1008	3323	3.25	1.834	2719	1.339	2221	1.450	2.716	0.987	0.701	1838	0.1227
1014	3280	3.19	1.812	2692	1.327	2193	1.433	2.478	.987	.781	1804	.1175
1002	3207	3.17	1.785	2631	1.306	2141	1.405	2.275	.987	.863	1832	.1211
1012	2970	2.98	1.649	2491	1.255	1995	1.340	2.157	.987	.842	1716	.1099
1010	2779	2.89	1.530	2383	1.205	1894	1.273	2.008	.987	.856	1661	.1062
1031	2418	2.75	1.341	2294	1.123	1798	1.163	1.909	.987	.716	1610	.1043

NACA

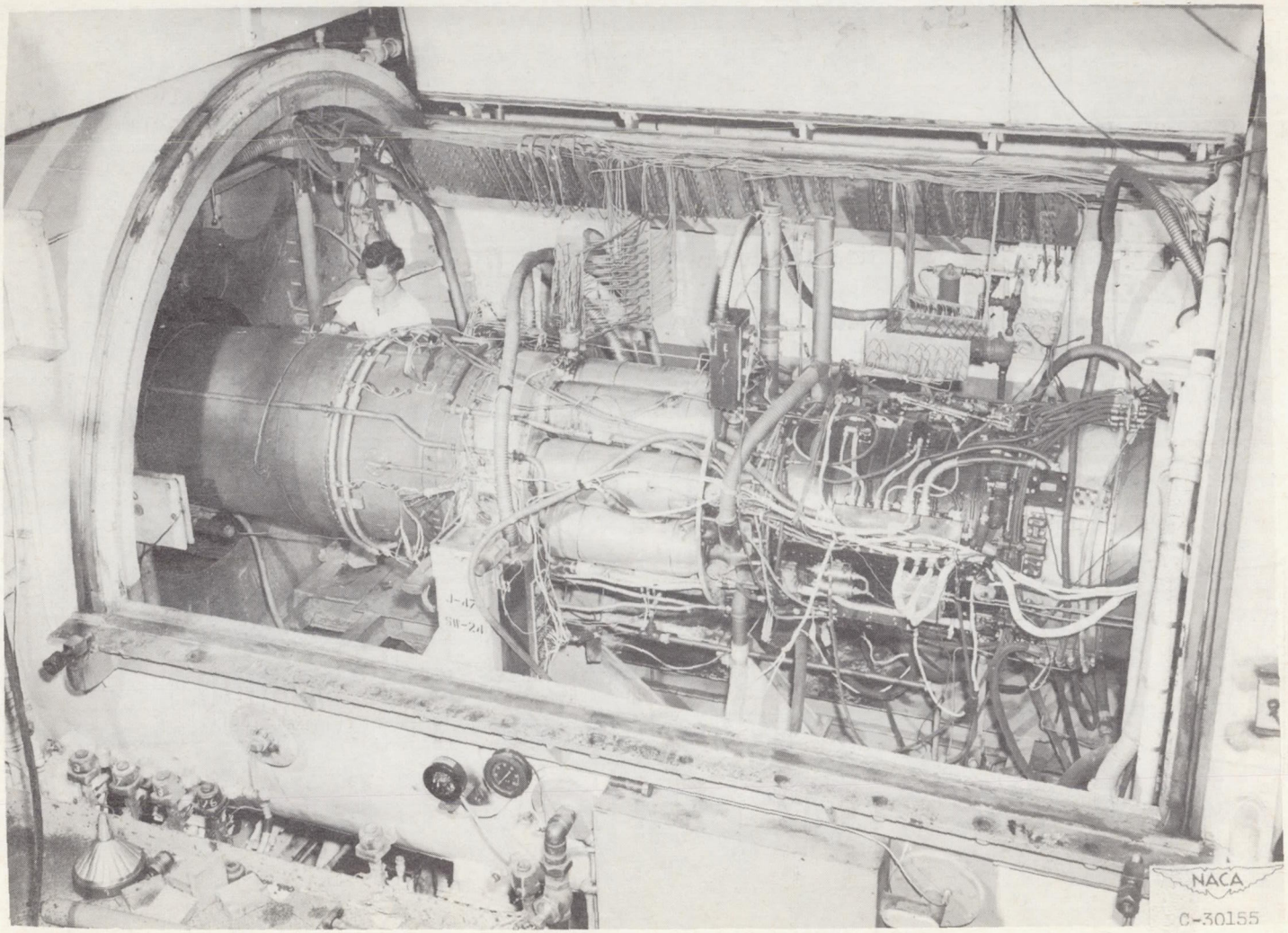

(a) Photograph of installation.

Figure 1. - Turbojet engine equipped with afterburner and installed in altitude chamber.

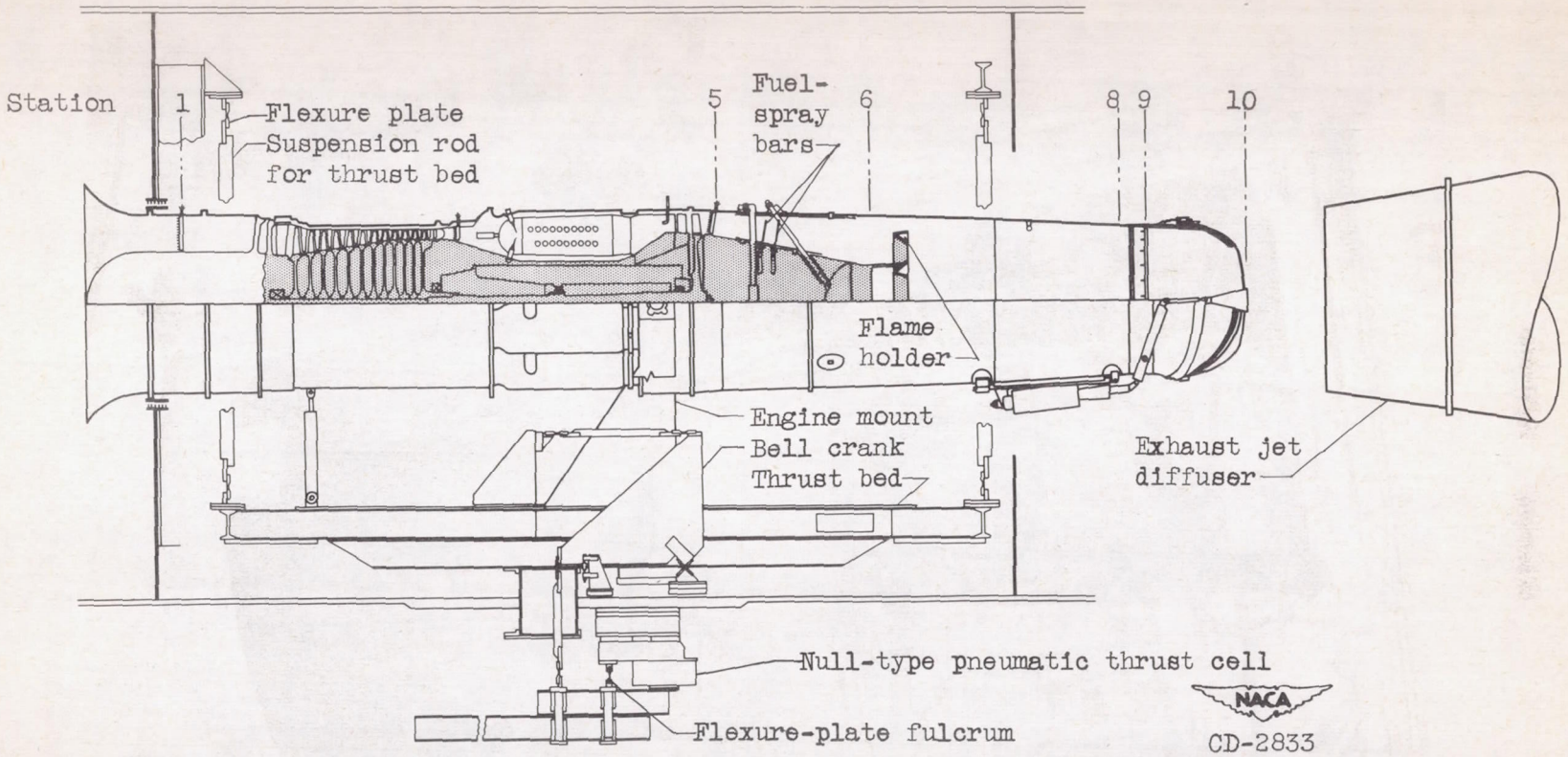

(b) Schematic diagram of engine installation showing thrust-measuring system and instrumentation stations.

Figure 1. - Concluded. Turbojet engine equipped with afterburner and installed in altitude chamber.

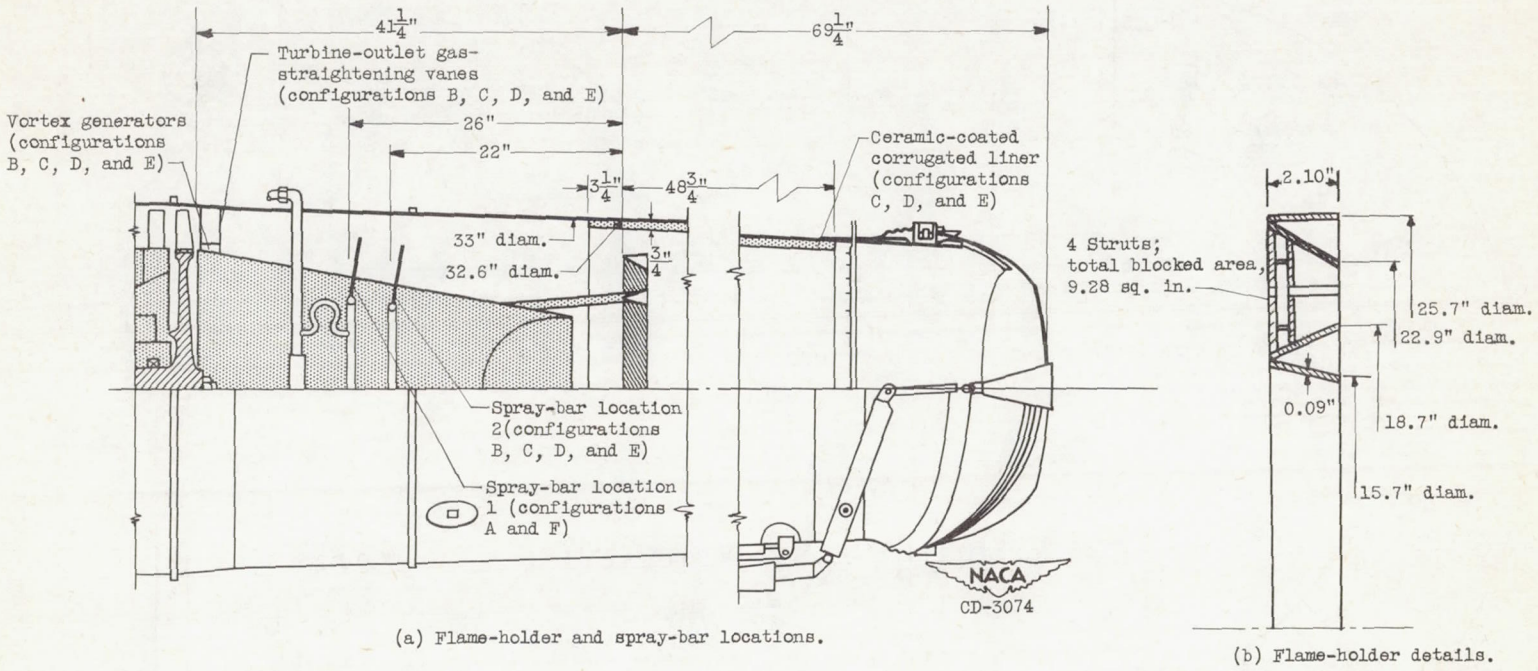

(a) Flame-holder and spray-bar locations.

(b) Flame-holder details.

Figure 2. - Diagram of afterburner showing location of spray bars and flame holder.

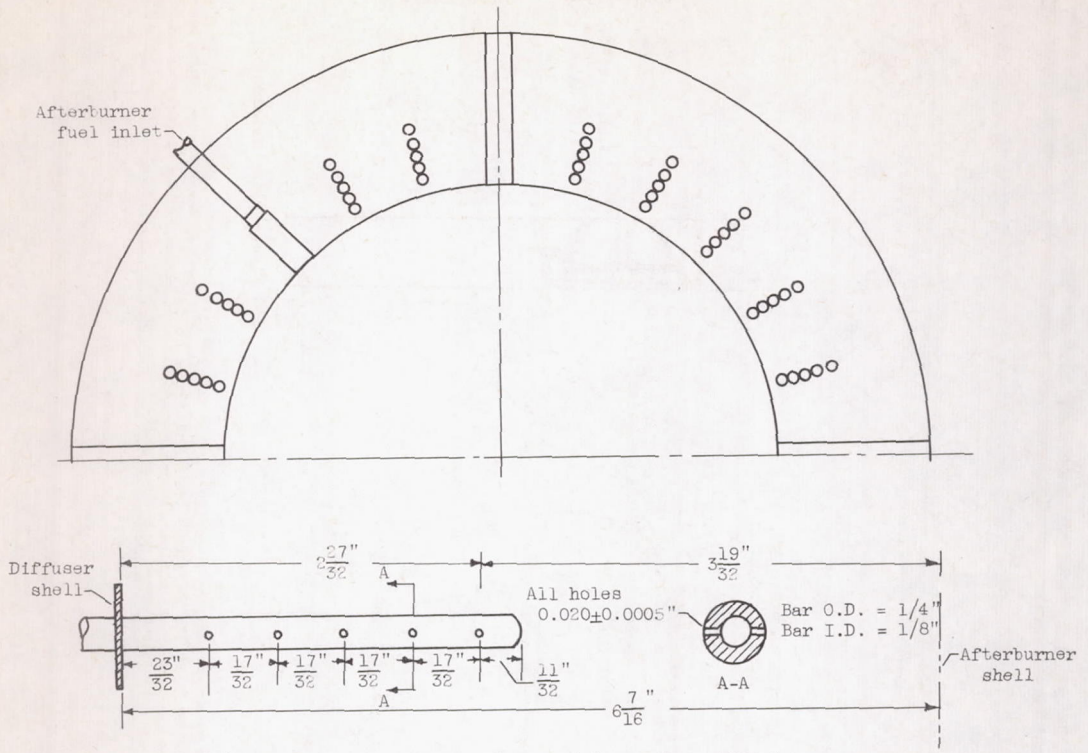

(a) Spray pattern and spray bar used in configuration A.

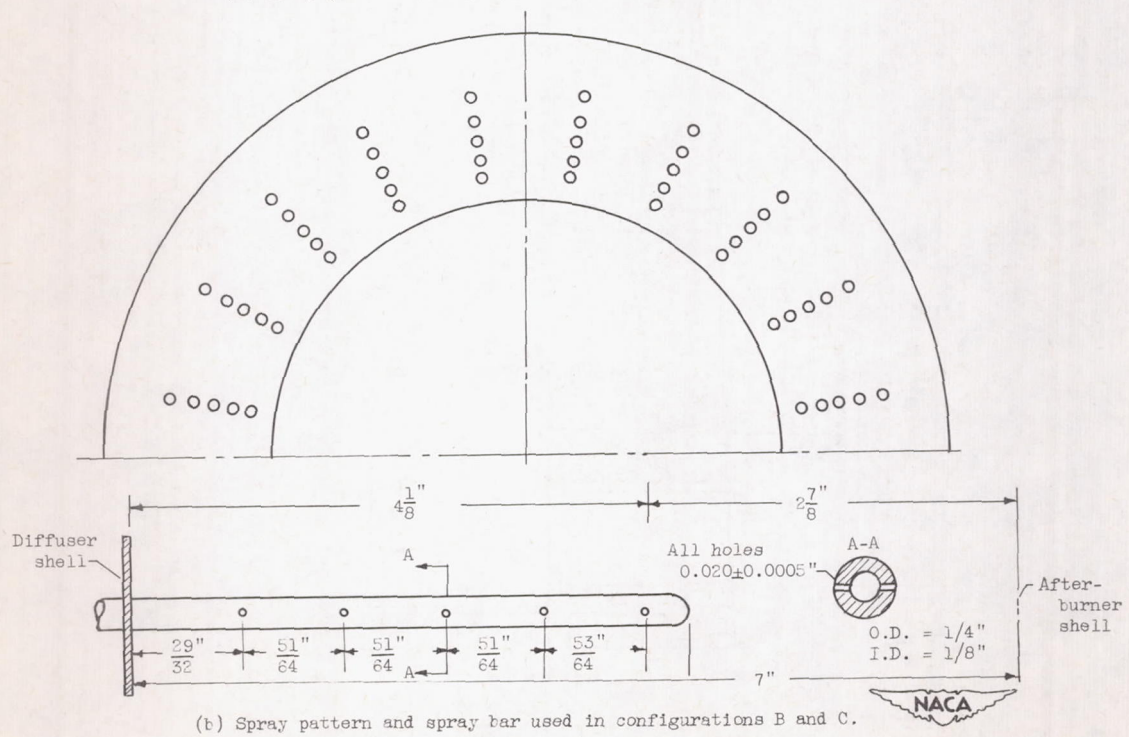

(b) Spray pattern and spray bar used in configurations B and C.

Figure 3. - Fuel-distribution patterns and spray-bar designs.

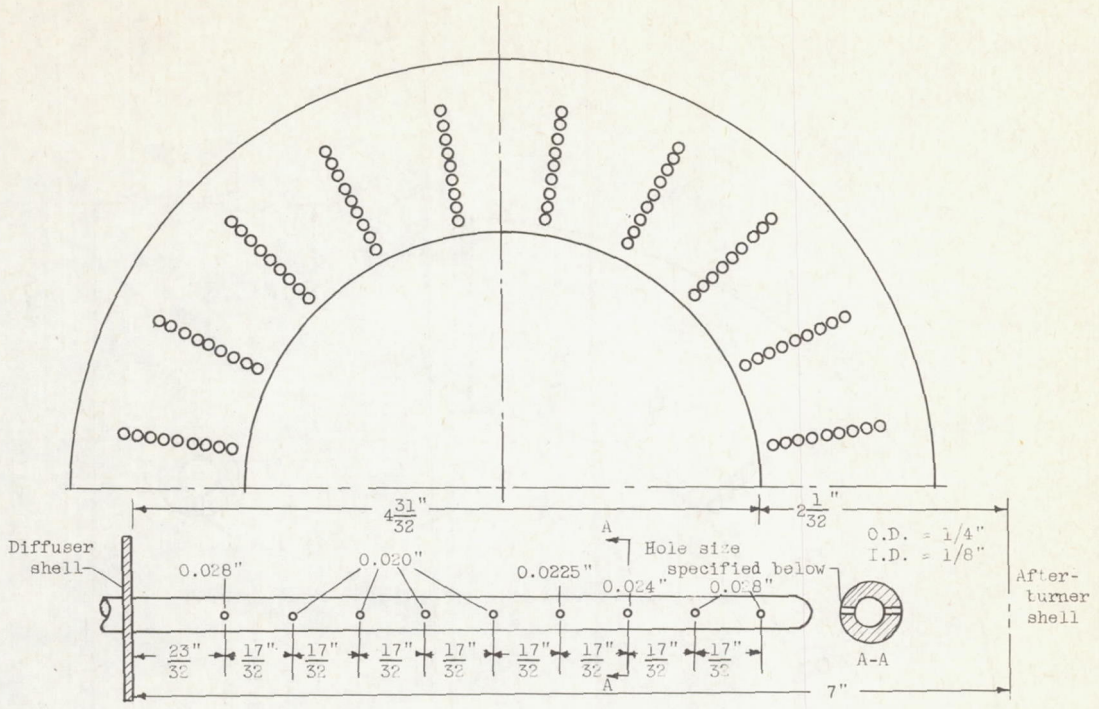

(c) Spray pattern and spray bar used in configuration D.

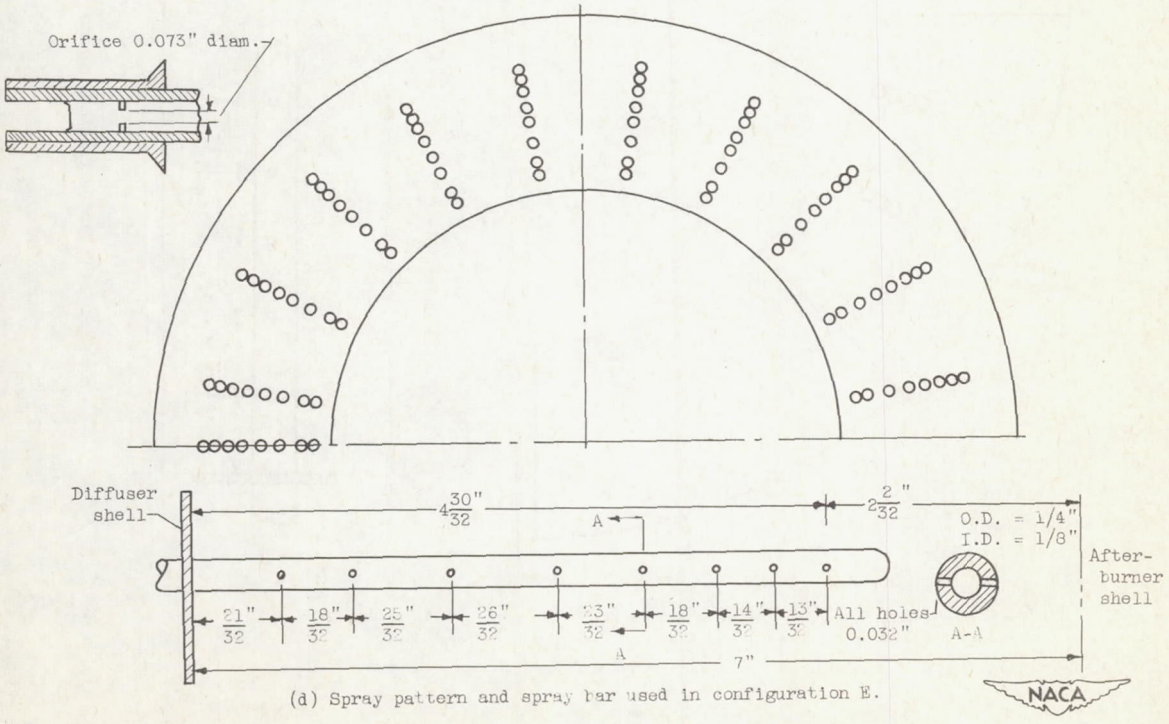

(d) Spray pattern and spray bar used in configuration E.

Figure 3. - Continued. Fuel-distribution patterns and spray-bar designs.

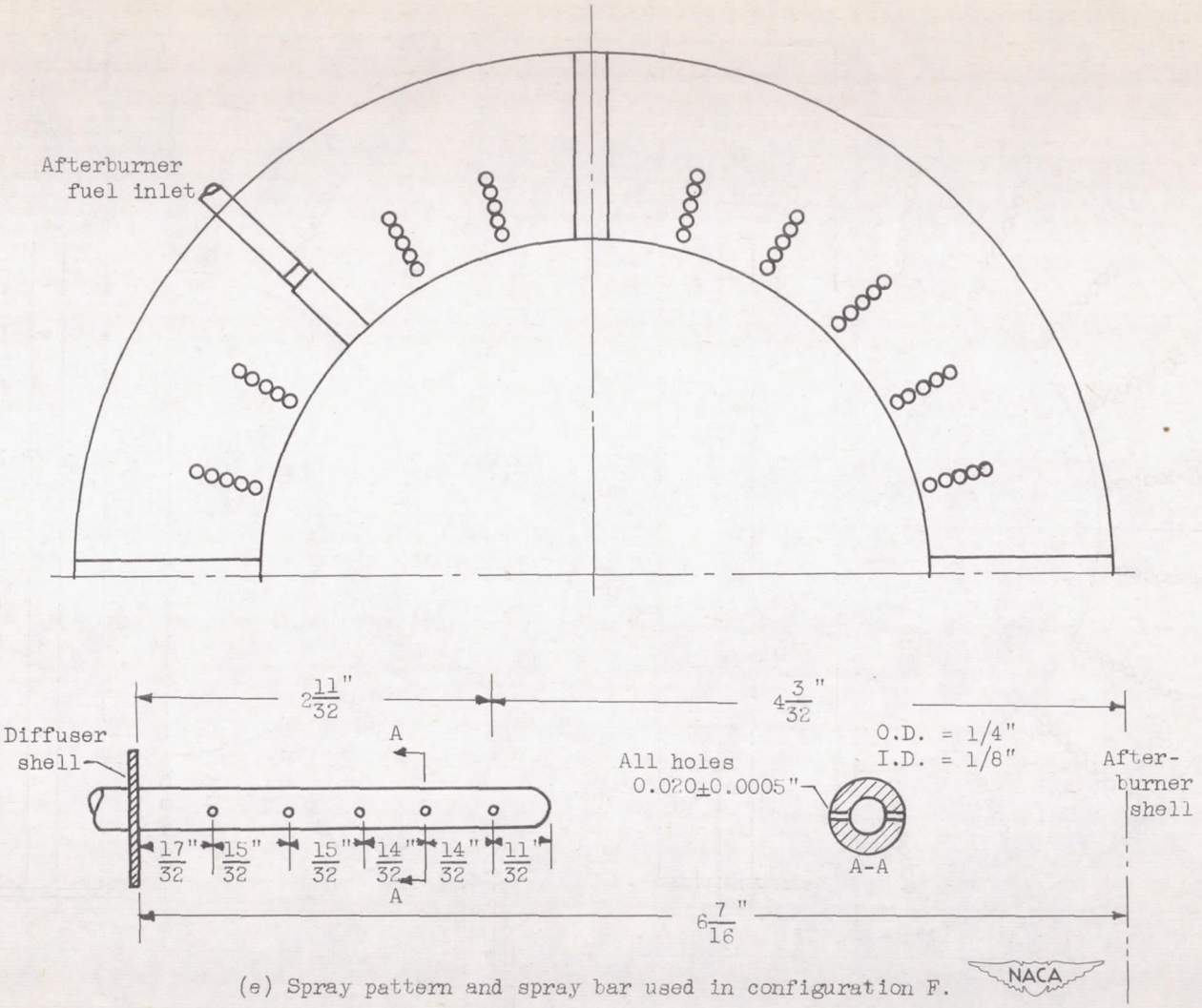

(e) Spray pattern and spray bar used in configuration F.

Figure 3. - Concluded. Fuel-distribution patterns and spray-bar designs.

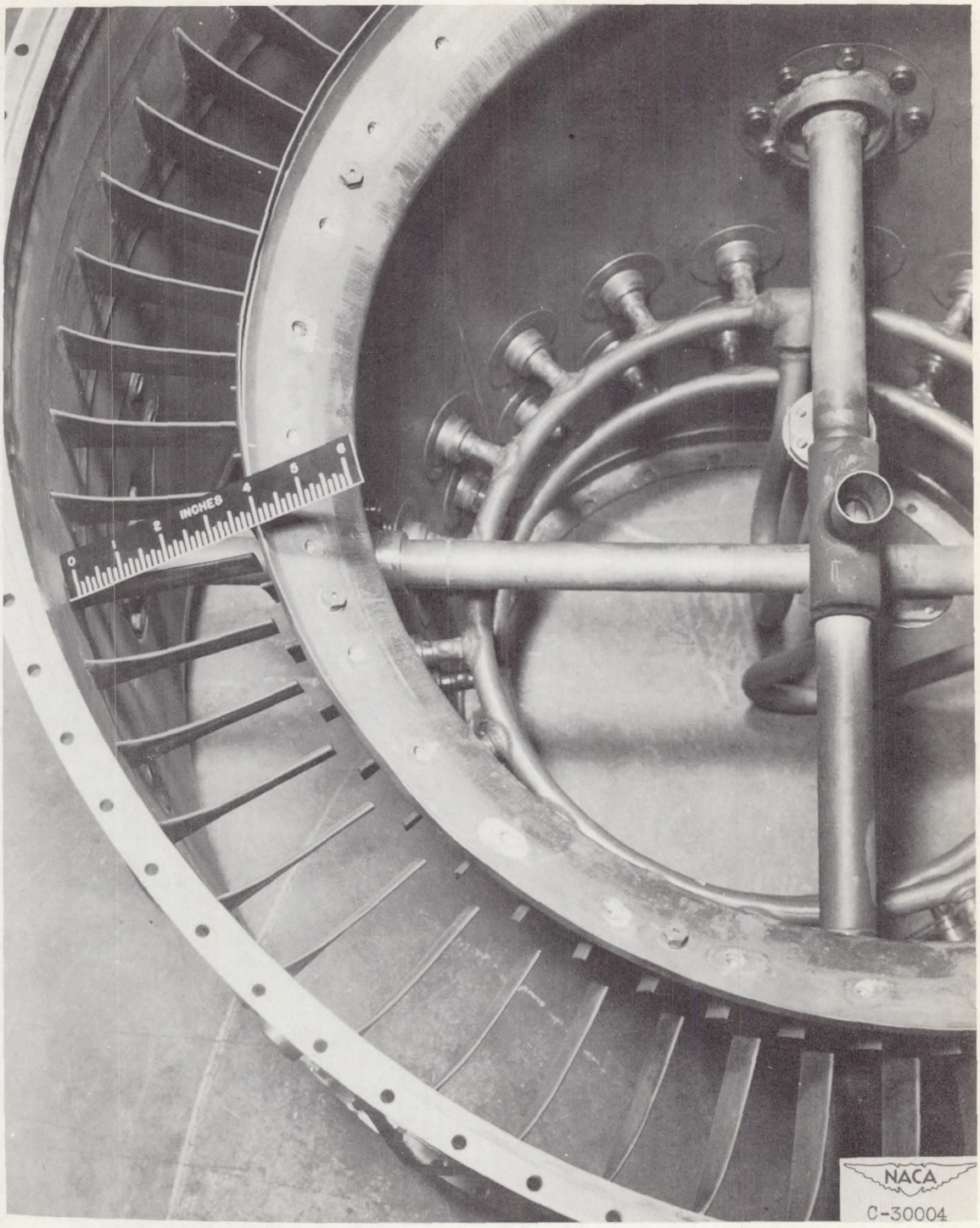

Figure 4. - Turbine-outlet gas-straightening vanes, vortex generators, and internal manifolds for configurations B, C, D, and E, as viewed in downstream direction.

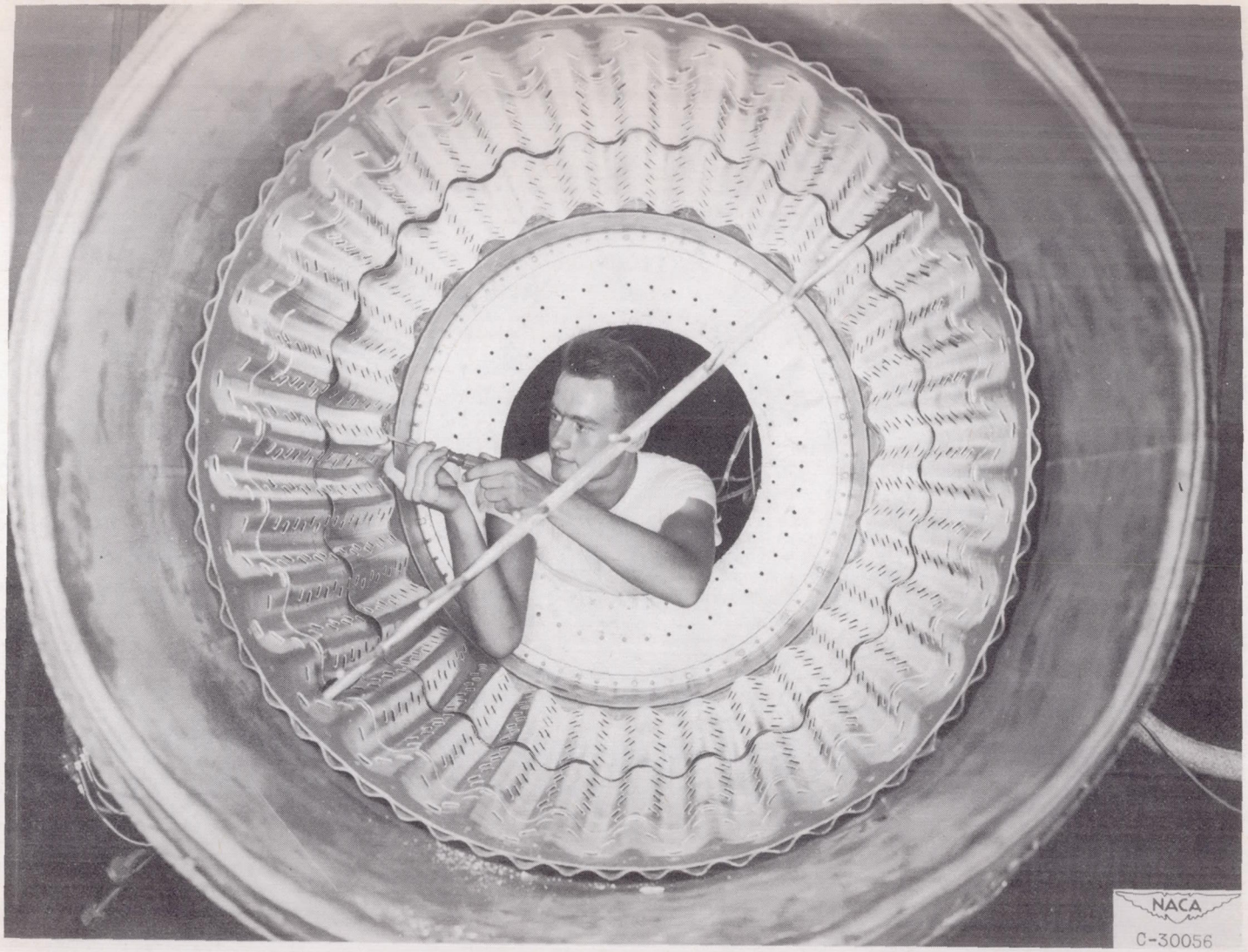

Figure 5. - Ceramic-coated corrugated liner installed in afterburner for configurations C, D, and E, as viewed in upstream direction.

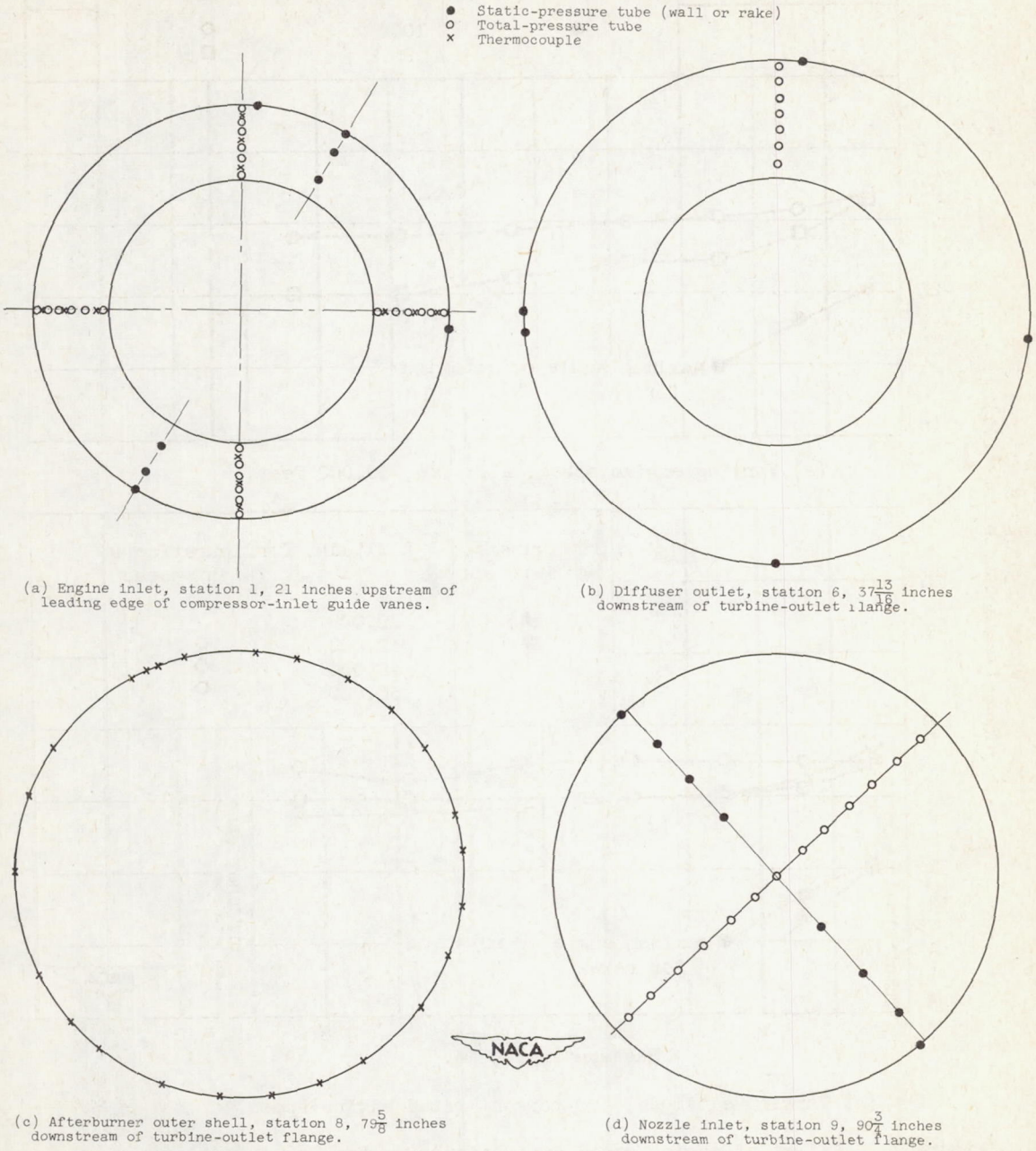

(a) Engine inlet, station 1, 21 inches upstream of leading edge of compressor-inlet guide vanes.

(b) Diffuser outlet, station 6, $37\frac{13}{16}$ inches downstream of turbine-outlet flange.

(c) Afterburner outer shell, station 8, $79\frac{5}{8}$ inches downstream of turbine-outlet flange.

(d) Nozzle inlet, station 9, $90\frac{3}{4}$ inches downstream of turbine-outlet flange.

Figure 6. - Instrumentation.

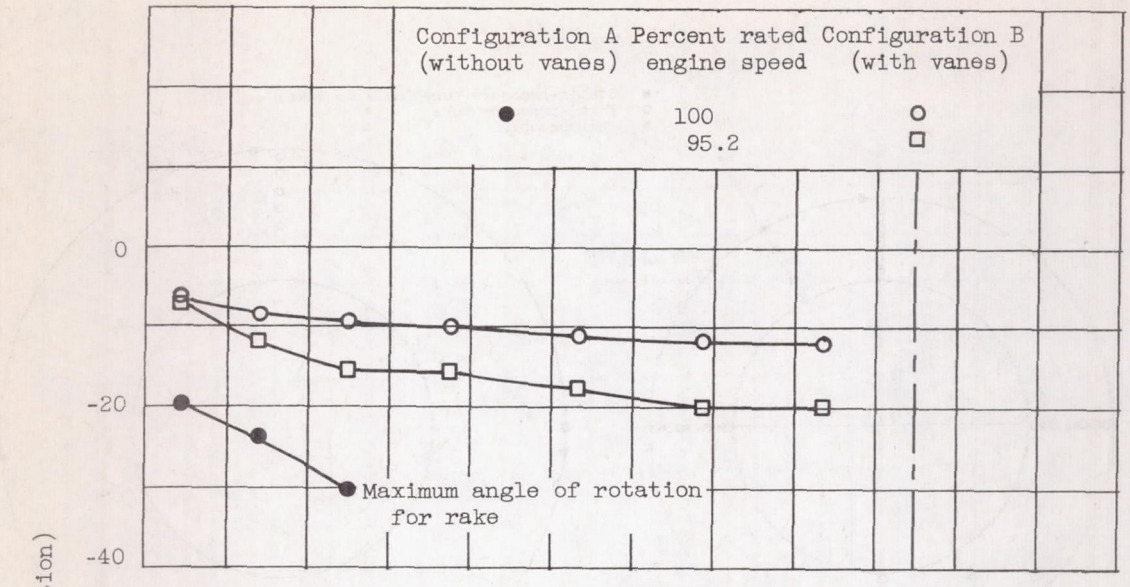

(a) Varying engine speed; altitude, 30,000 feet.

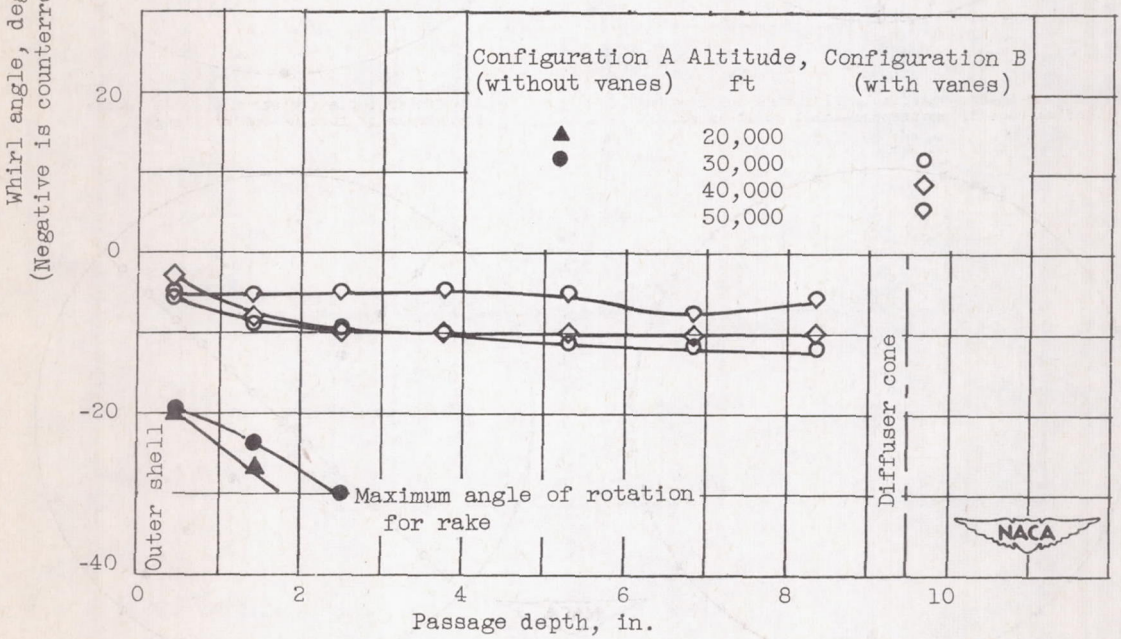

(b) Varying altitude; 100-percent rated engine speed.

Figure 7. - Effect of engine speed and altitude on turbine-outlet gas whirl at flight Mach number of 0.6.

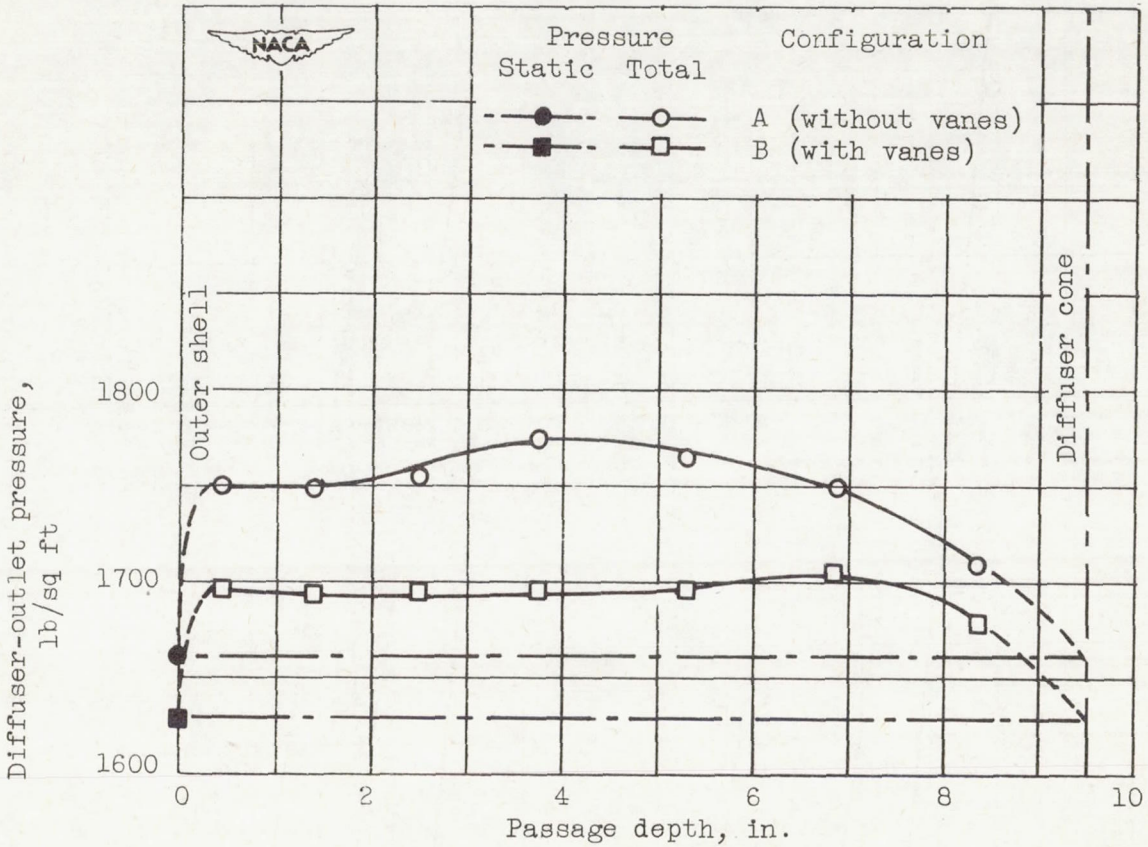

Figure 8. - Effect of turbine-outlet straightening vanes and vortex generators on diffuser-outlet total-pressure profile. Altitude, 30,000 feet; flight Mach number, 0.6.

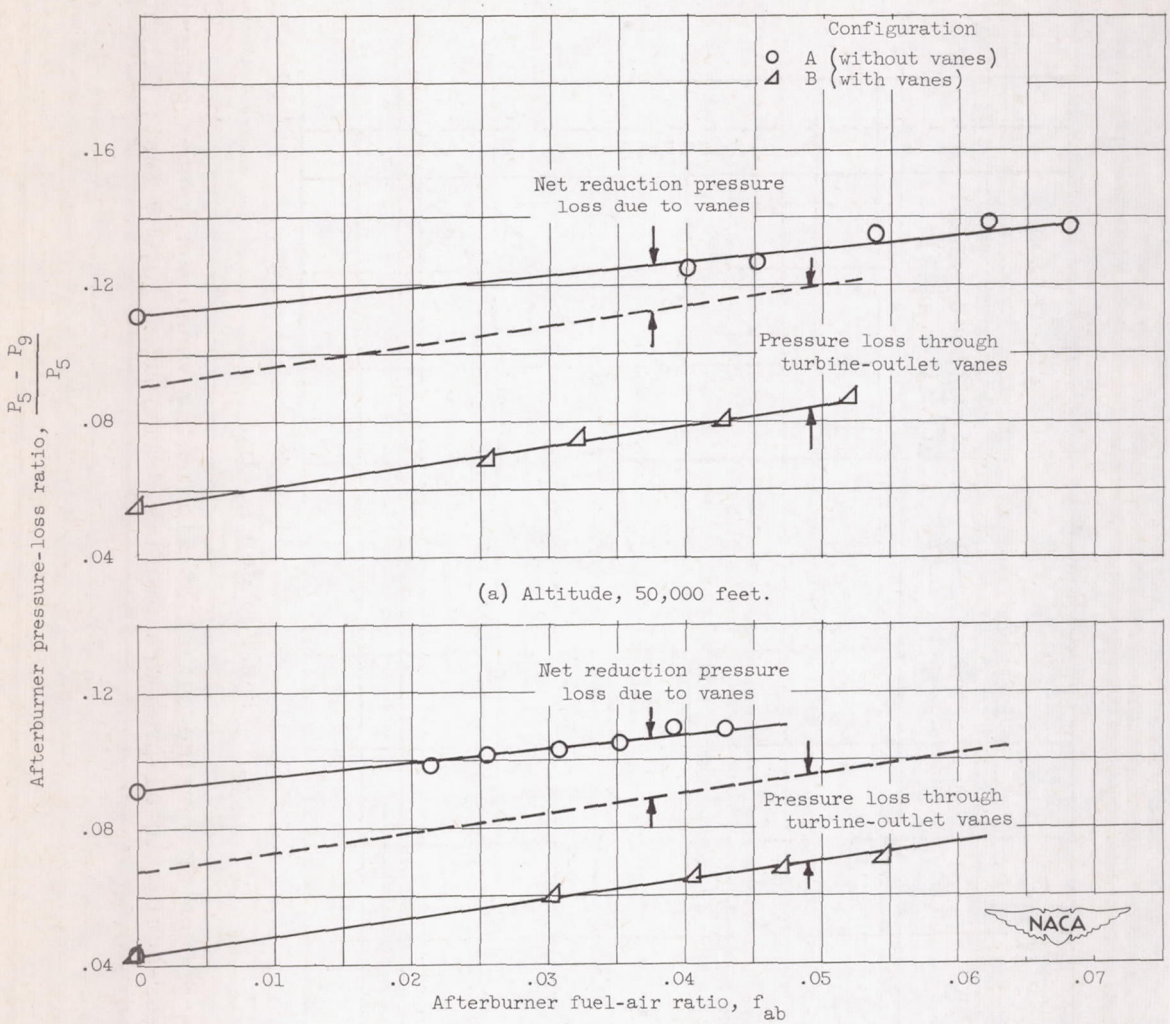

Figure 9 - Effect of turbine-outlet gas-straightening vanes, vortex generators, and corrugated liner on afterburner pressure loss. Flight Mach number, 0.6.

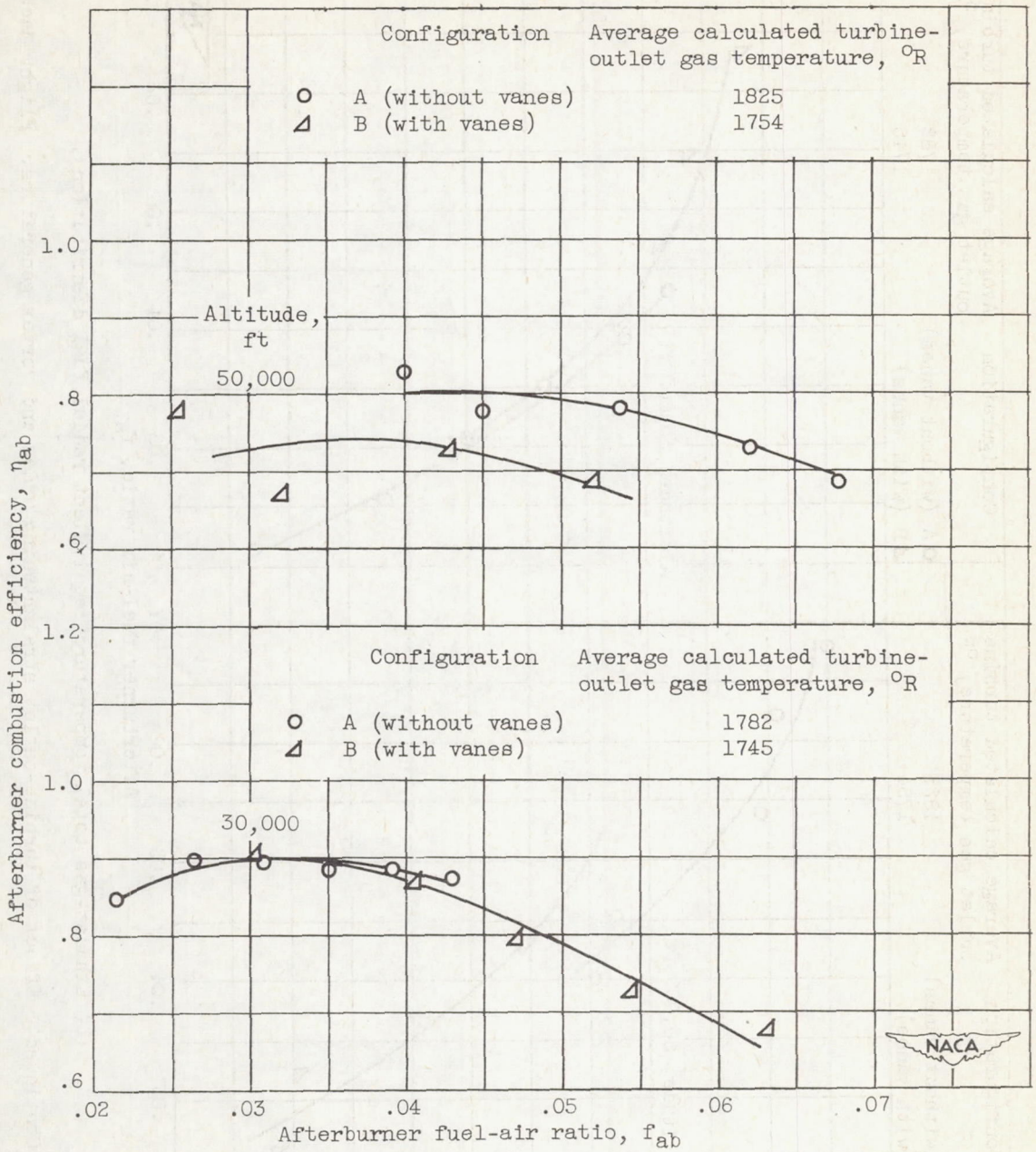

(a) Afterburner combustion efficiency (equivalent radial fuel distribution).

Figure 10. - Effect of turbine-outlet straightening vanes and vortex generators. Flight Mach number, 0.6.

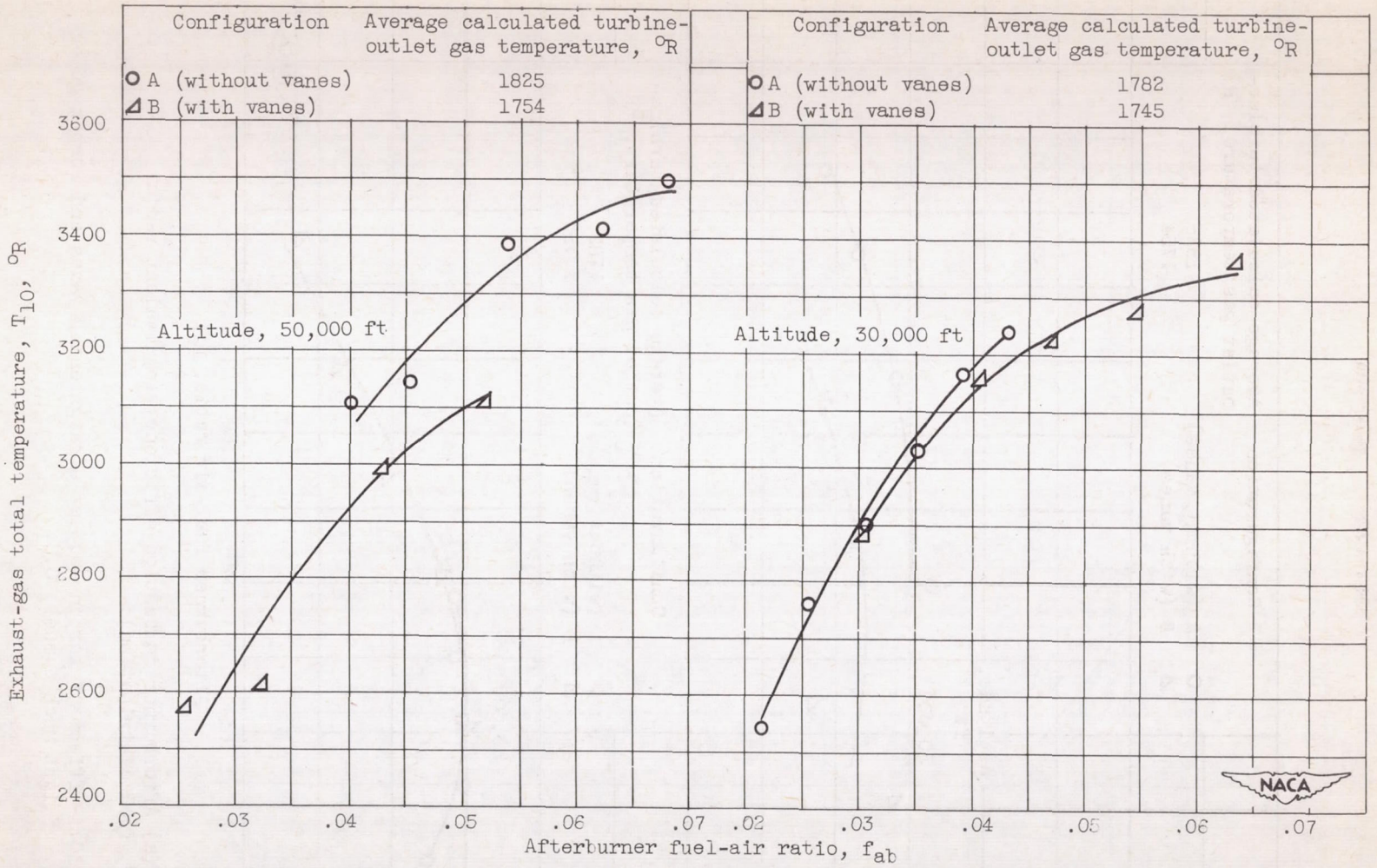

(b) Exhaust-gas total temperature (equivalent radial fuel distribution).

Figure 10. - Continued. Effect of turbine-outlet straightening vanes and vortex generators. Flight Mach number, 0.8.

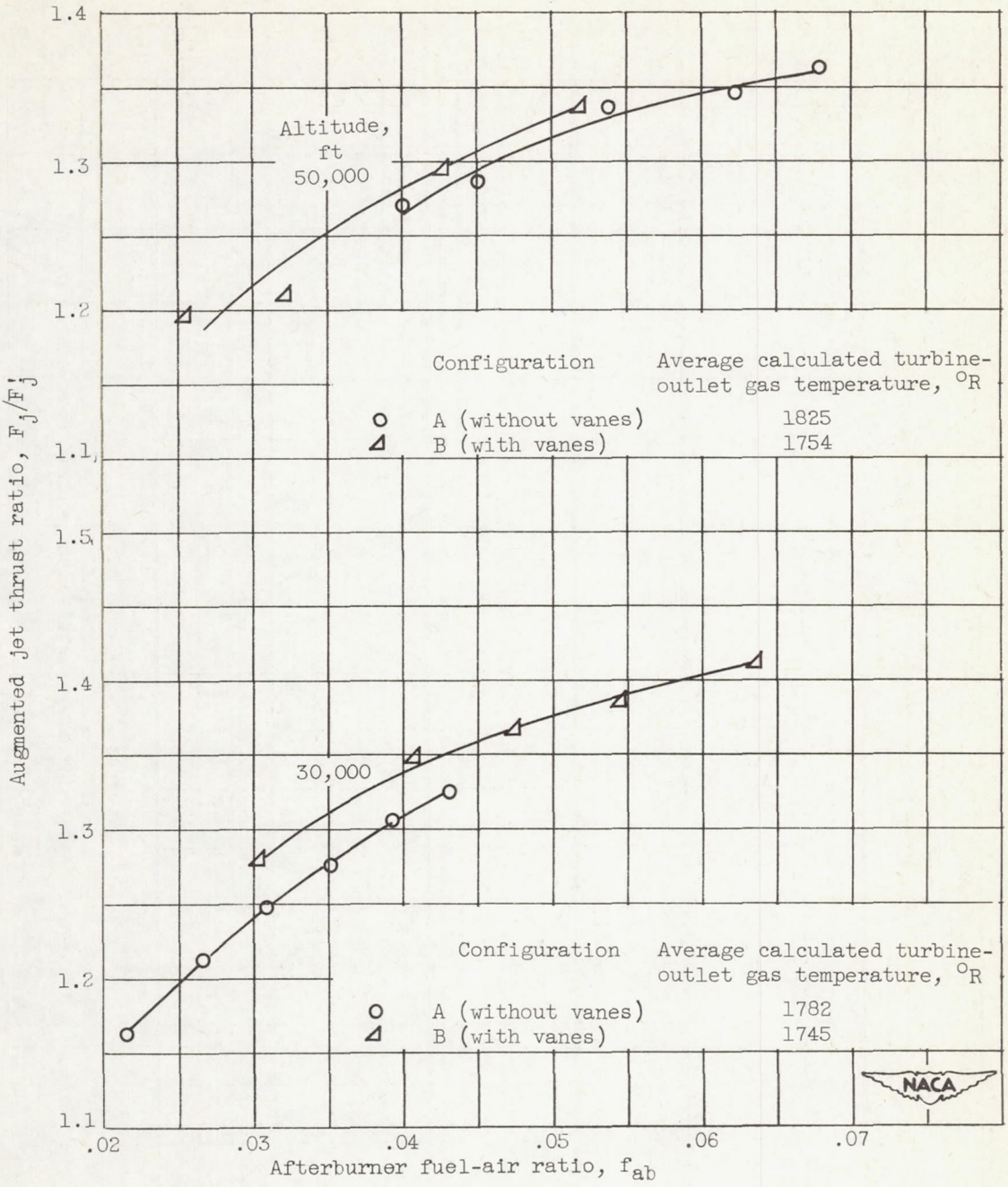

(c) Augmented jet thrust ratio (equivalent radial fuel distribution).

Figure 10. - Continued. Effect of turbine-outlet straightening vanes and vortex generators. Flight Mach number, 0.6.

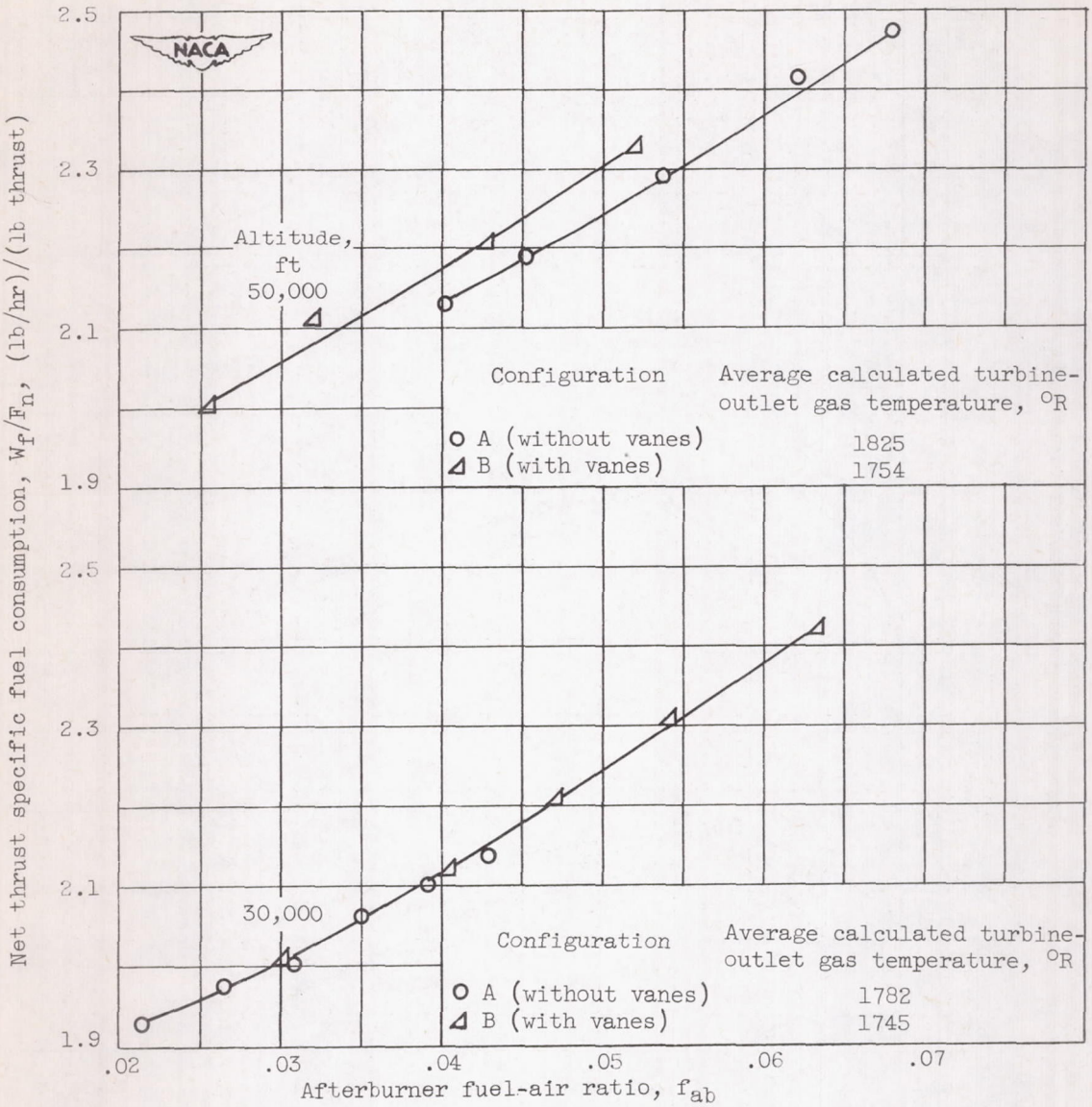

(d) Net thrust specific fuel consumption (equivalent radial fuel distribution).

Figure 10. - Concluded. Effect of turbine-outlet straightening vanes and vortex generators. Flight Mach number, 0.6.

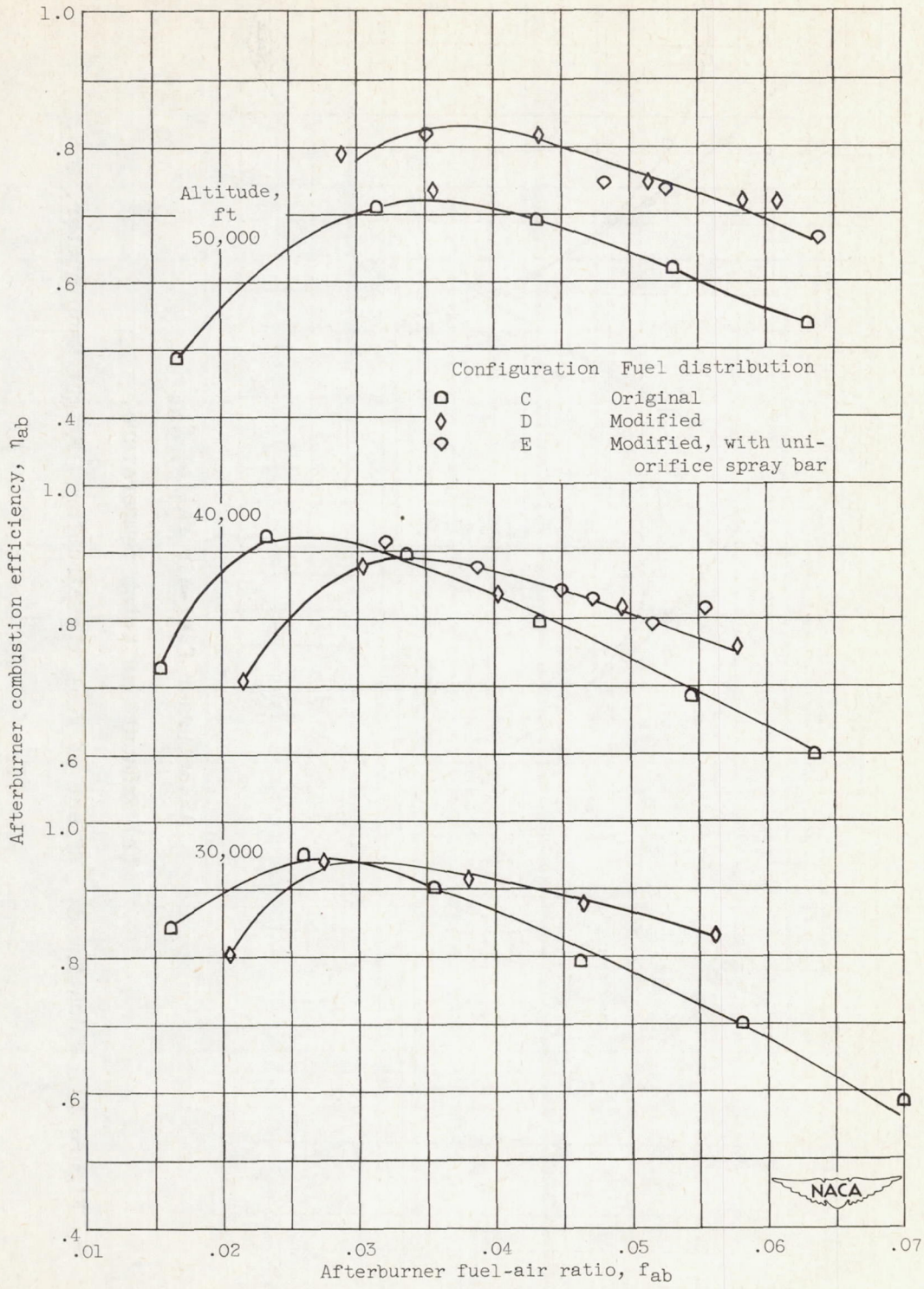

(a) Afterburner combustion efficiency.

Figure 11. - Effect of fuel distribution. Flight Mach number, 0.6.

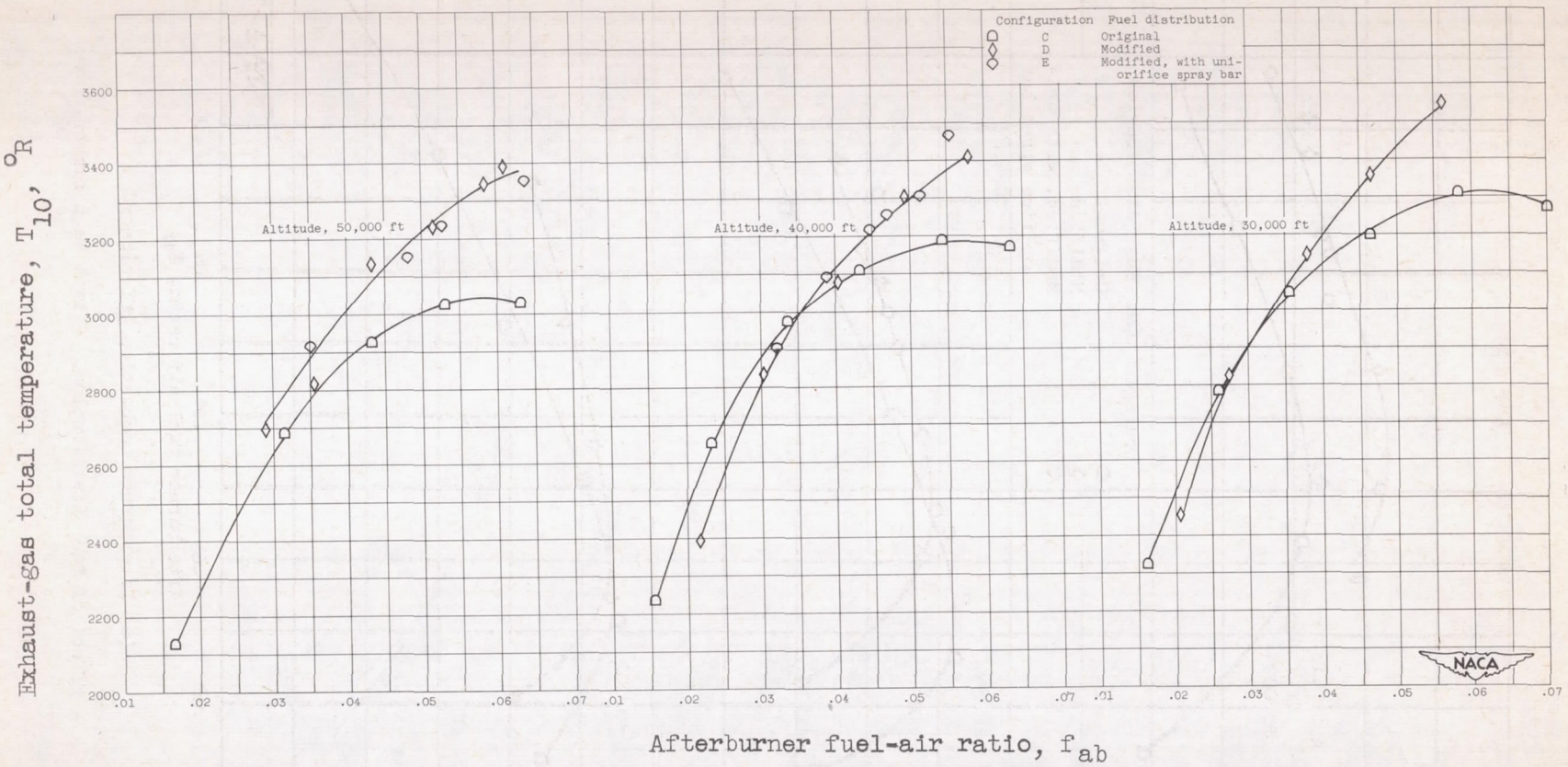

(b) Exhaust-gas total temperature.

Figure 11. - Continued. Effect of fuel distribution. Flight Mach number, 0.6.

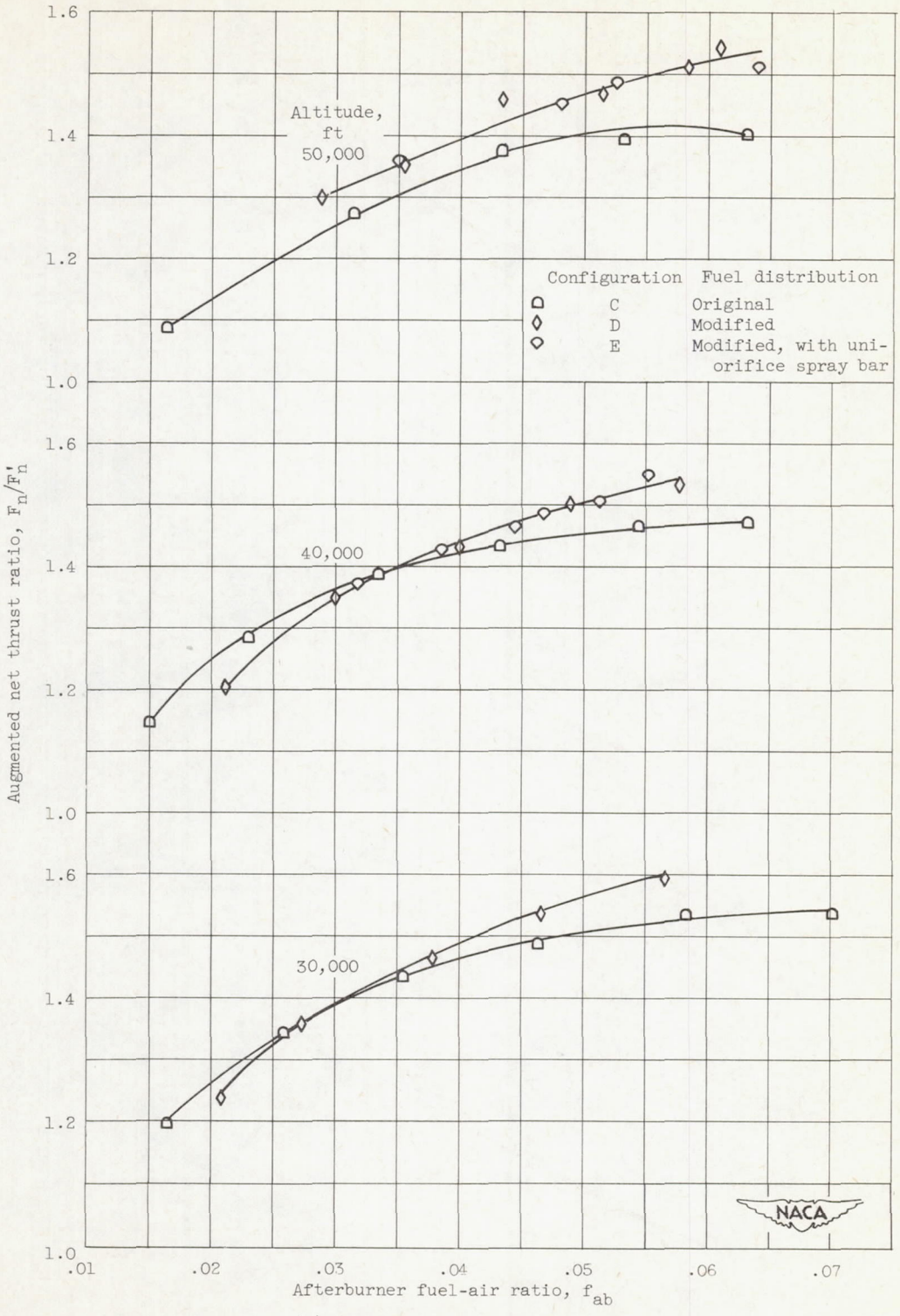

(c) Augmented net thrust ratio.

Figure 11. - Continued. Effect of fuel distribution. Flight Mach number, 0.6.

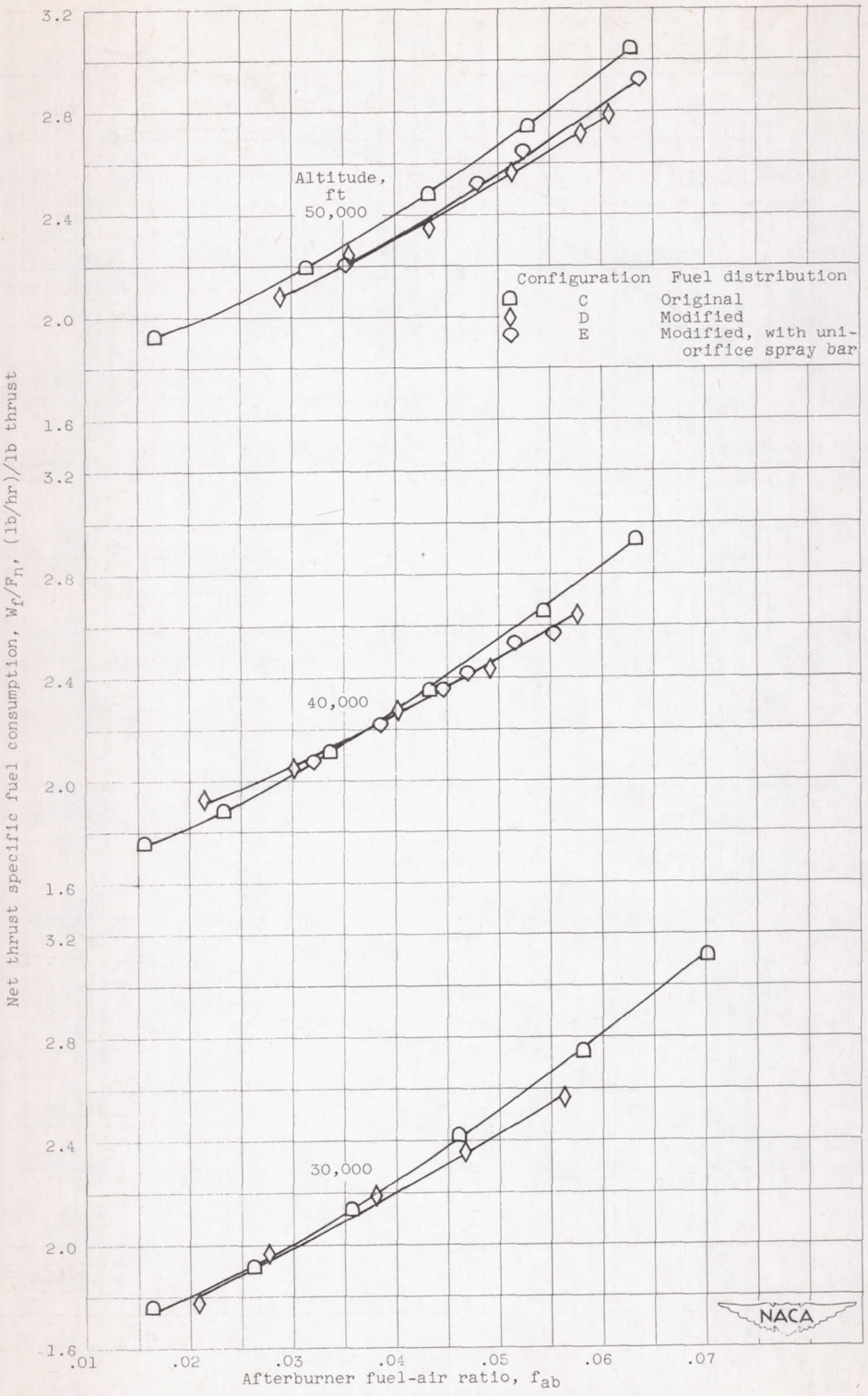

(d) Net thrust specific fuel consumption.

Figure 11. - Concluded. Effect of fuel distribution. Flight Mach number, 0.6.

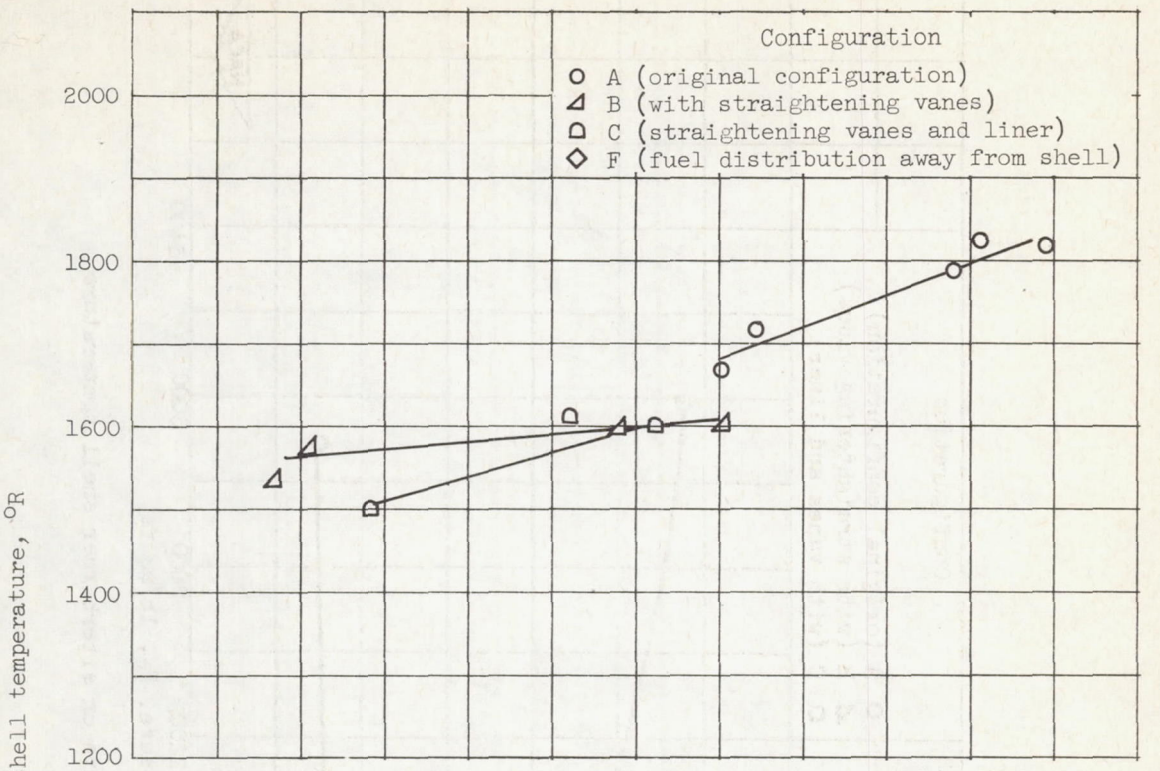

(a) Altitude, 50,000 feet.

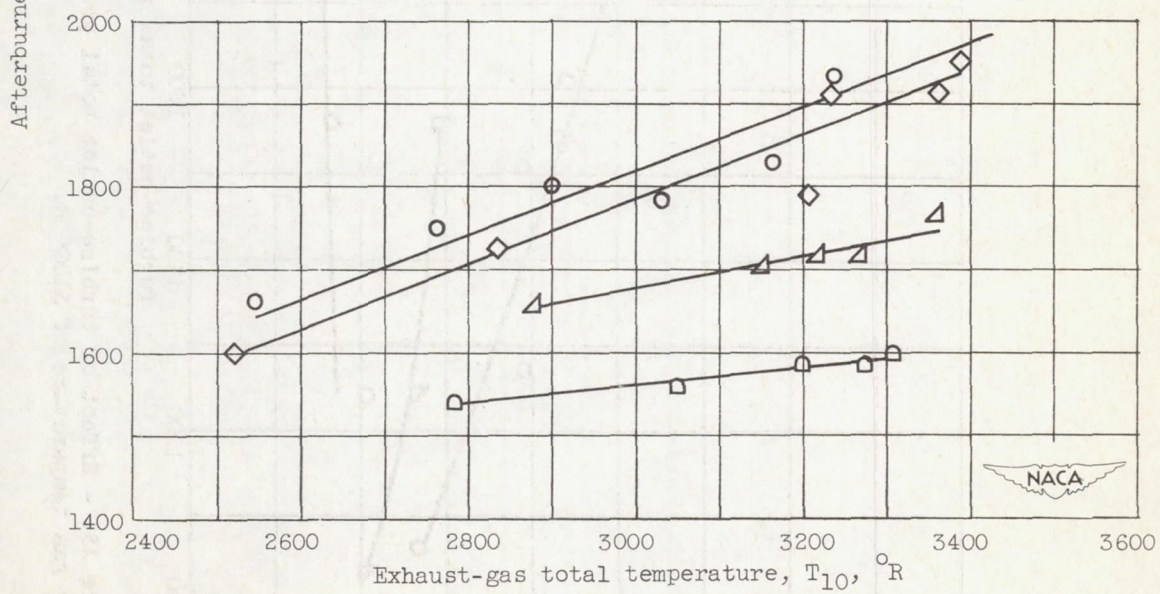

(b) Altitude, 30,000 feet.

Figure 12. - Effect of turbine-outlet gas-straightening vanes and vortex generators, ceramic-coated corrugated liner, and fuel distribution on afterburner shell temperature. Flight Mach number, 0.6.

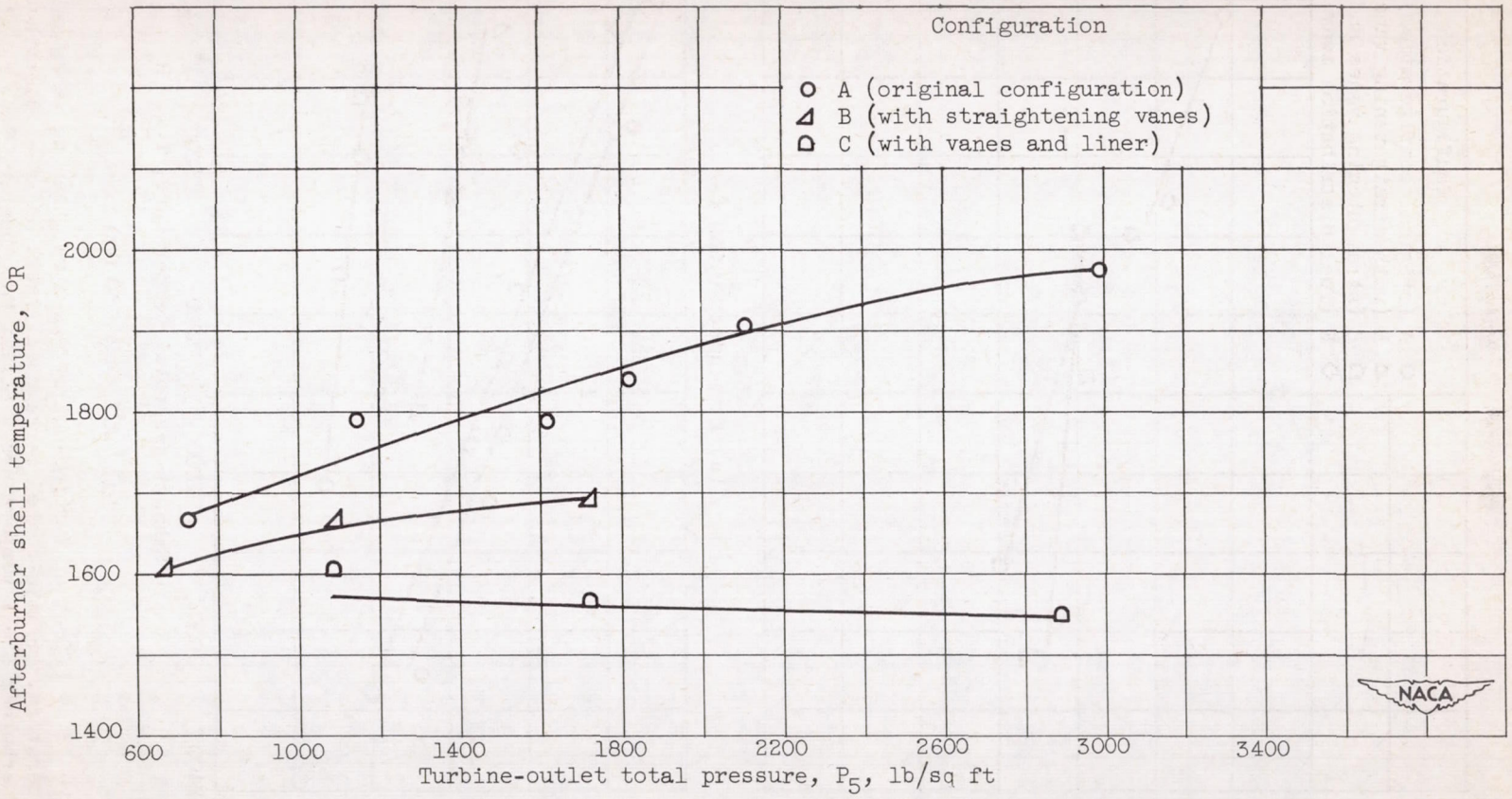

Figure 13. - Effect of turbine-outlet total pressure on afterburner shell temperature for gas temperature of 3100° R.

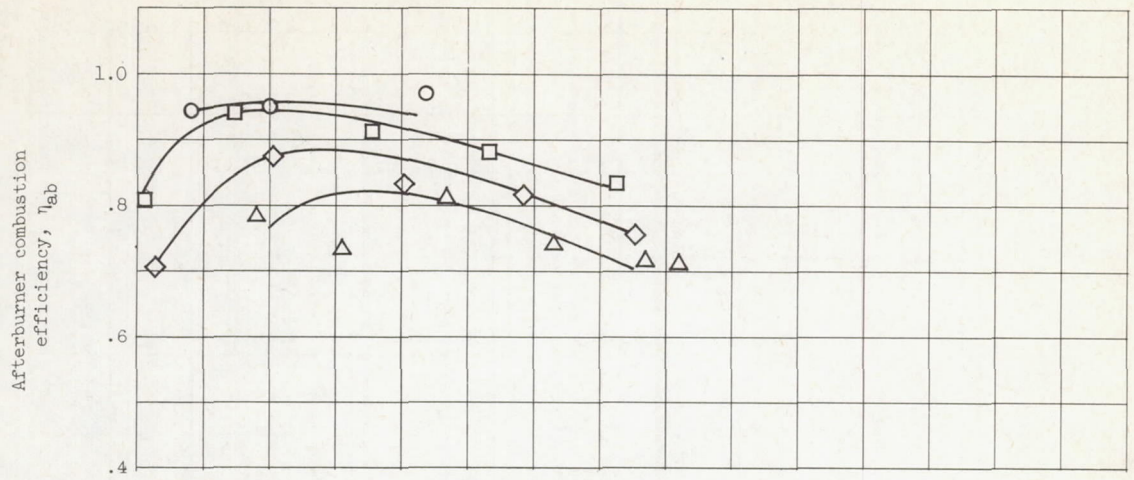

(a) Afterburner combustion efficiency.

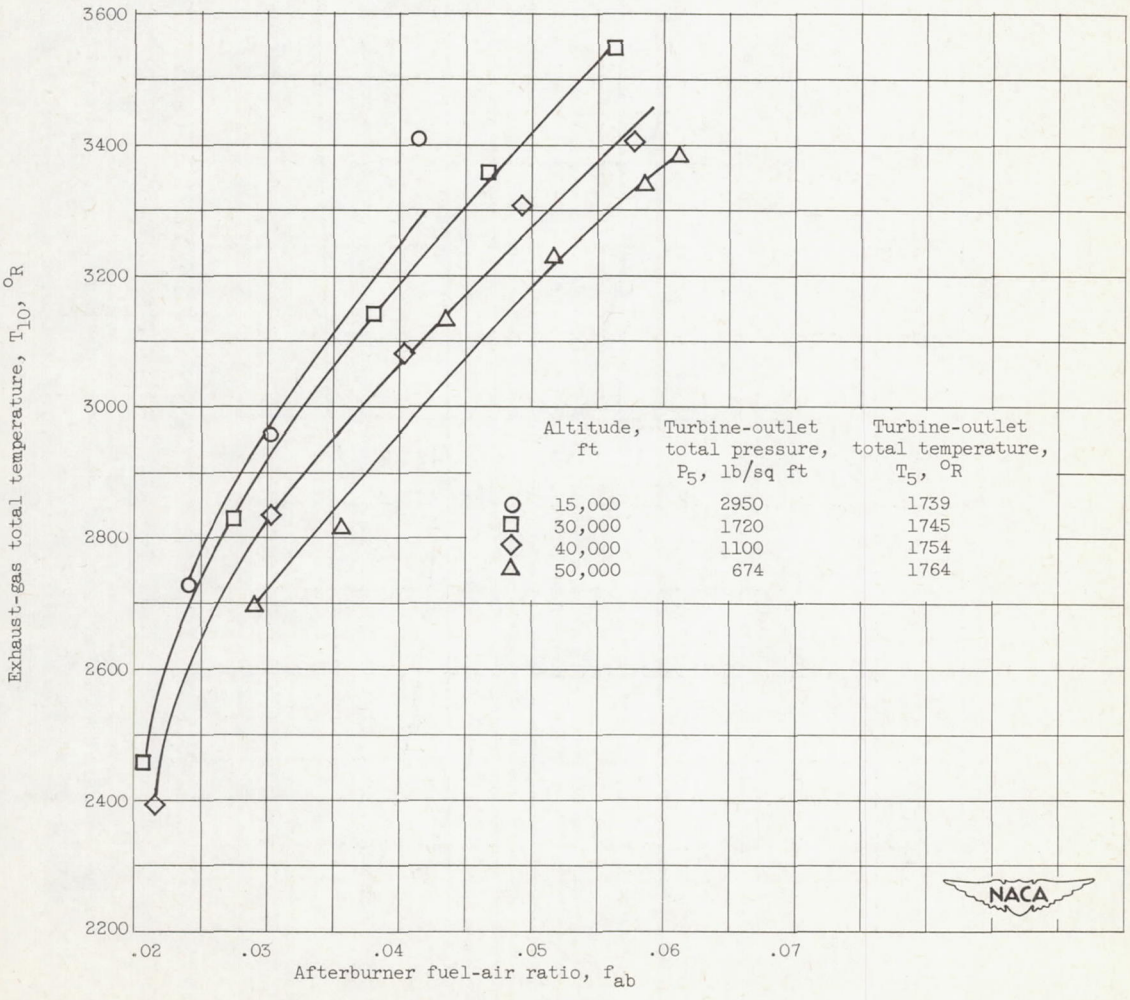

(b) Exhaust-gas total temperature.

Figure 14.- Effect of altitude on performance of configuration D. Flight Mach number, 0.6.

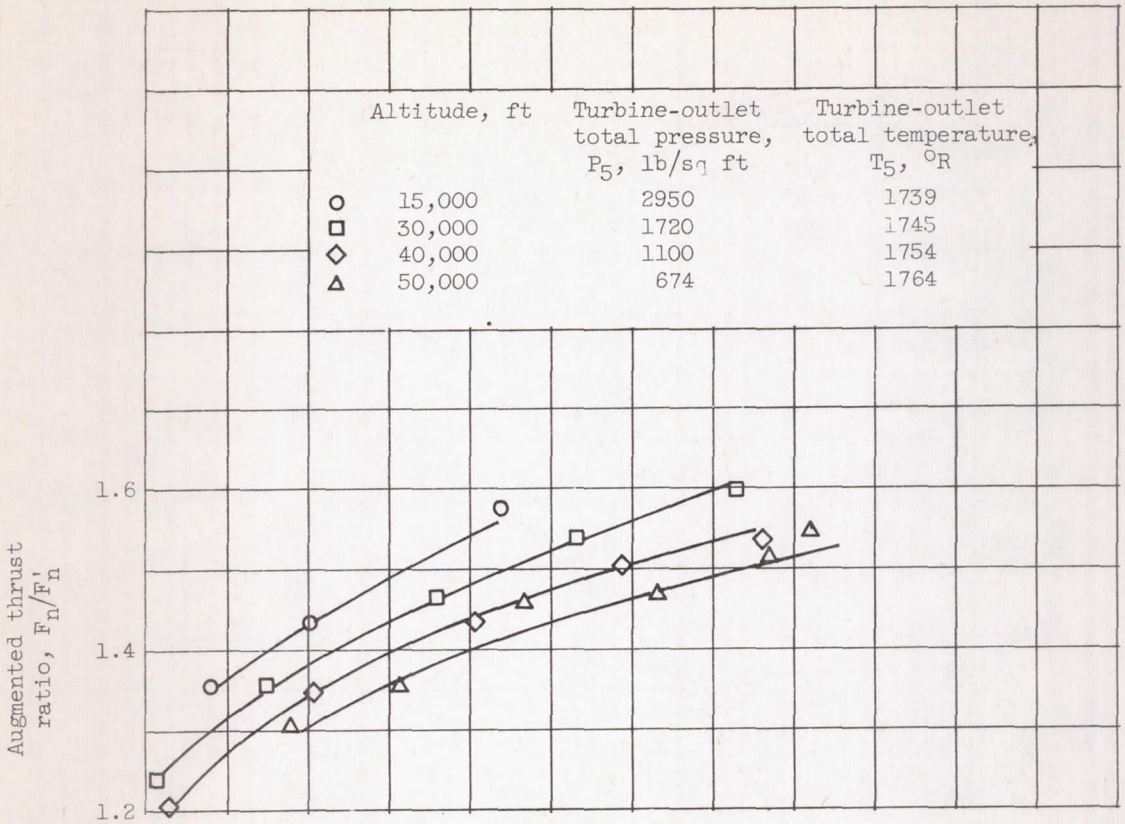

(c) Augmented thrust ratio.

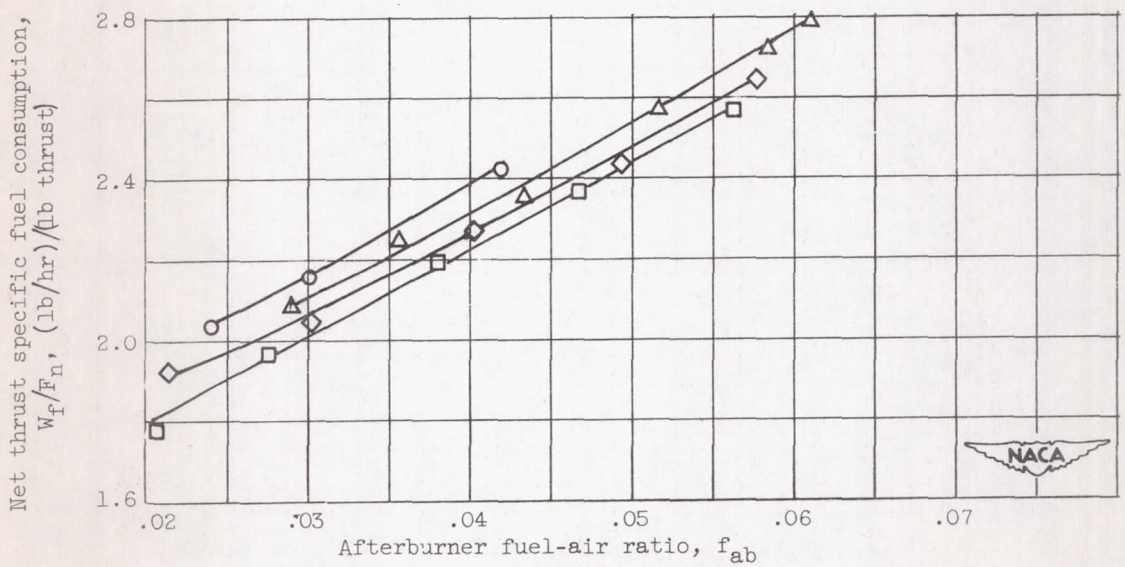

(d) Net thrust specific fuel consumption.

Figure 14. - Concluded. Effect of altitude on performance of configuration D. Flight Mach number, 0.6.

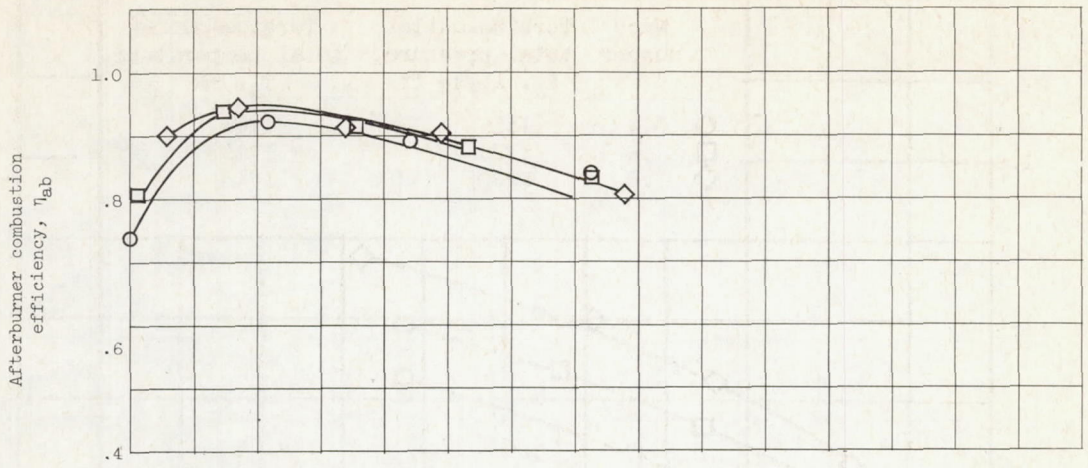

(a) Afterburner combustion efficiency.

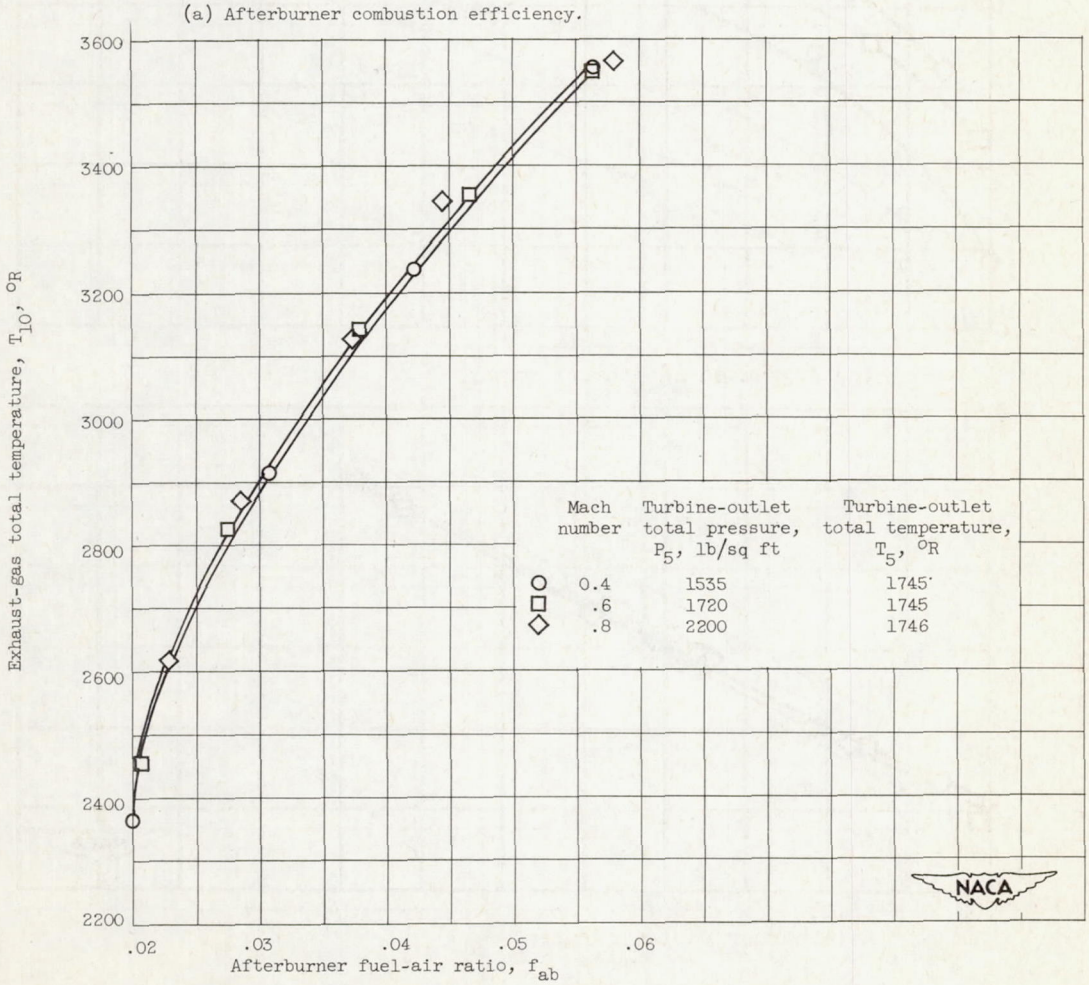

(b) Exhaust-gas total temperature.

Figure 15. - Effect of flight Mach number on performance of configuration D. Altitude, 30,000 feet.

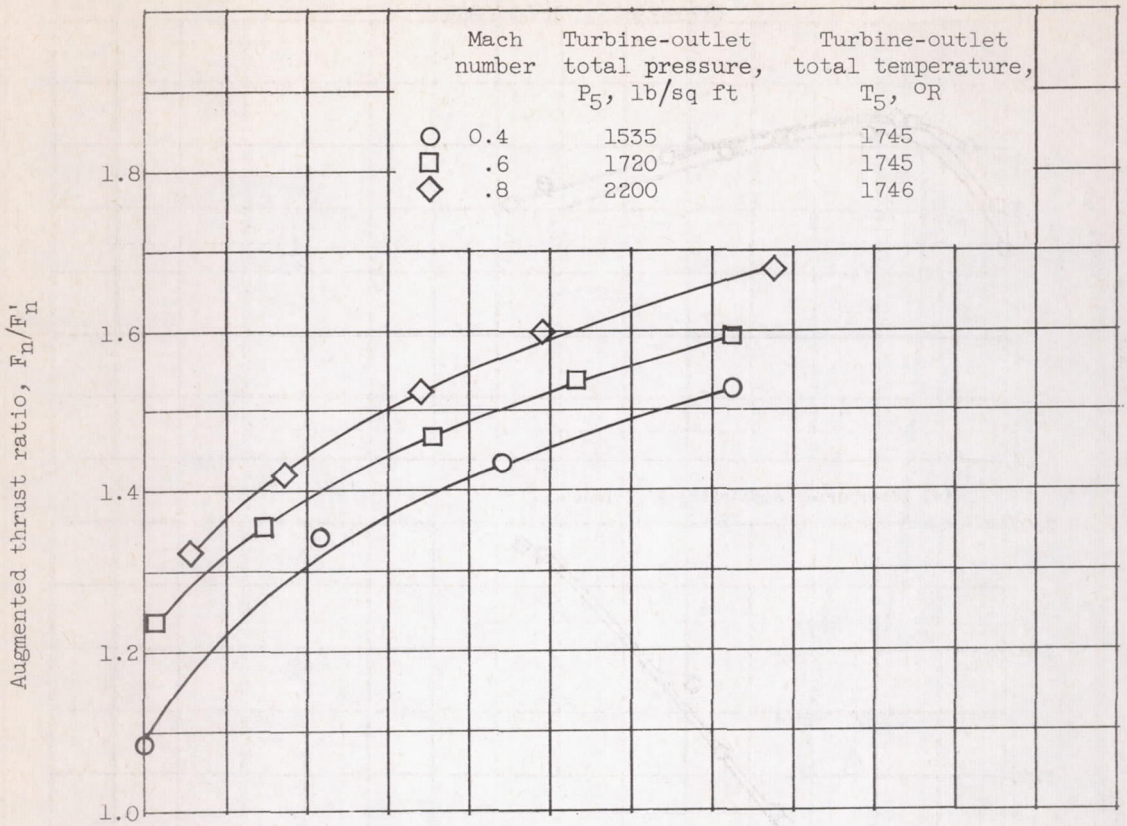

(c) Augmented net thrust ratio.

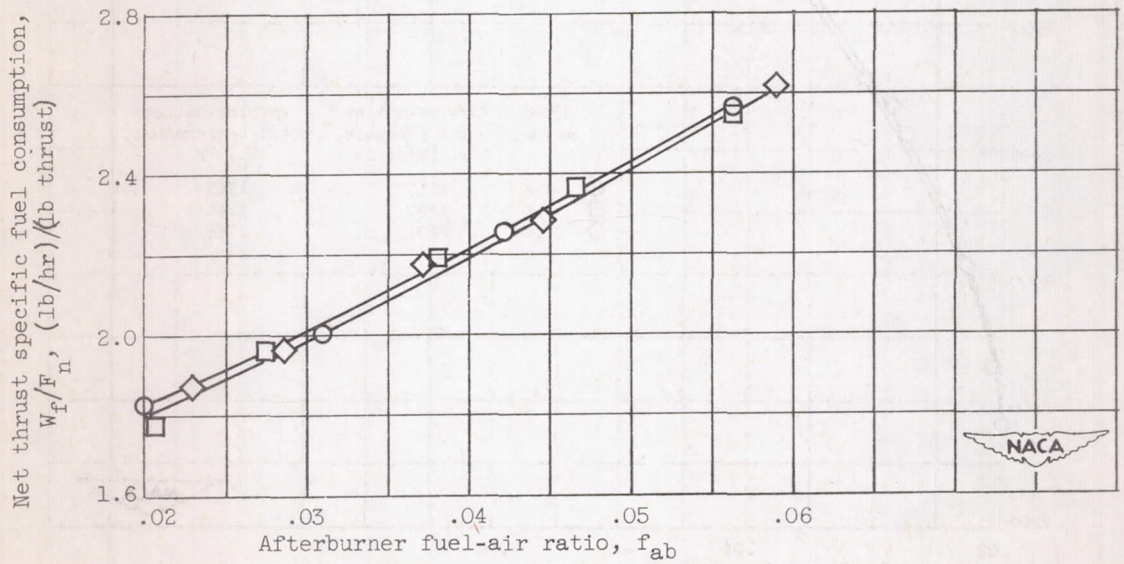

(d) Net thrust specific fuel consumption.

Figure 15. - Concluded. Effect of flight Mach number on performance of configuration D. Altitude, 30,000 feet.

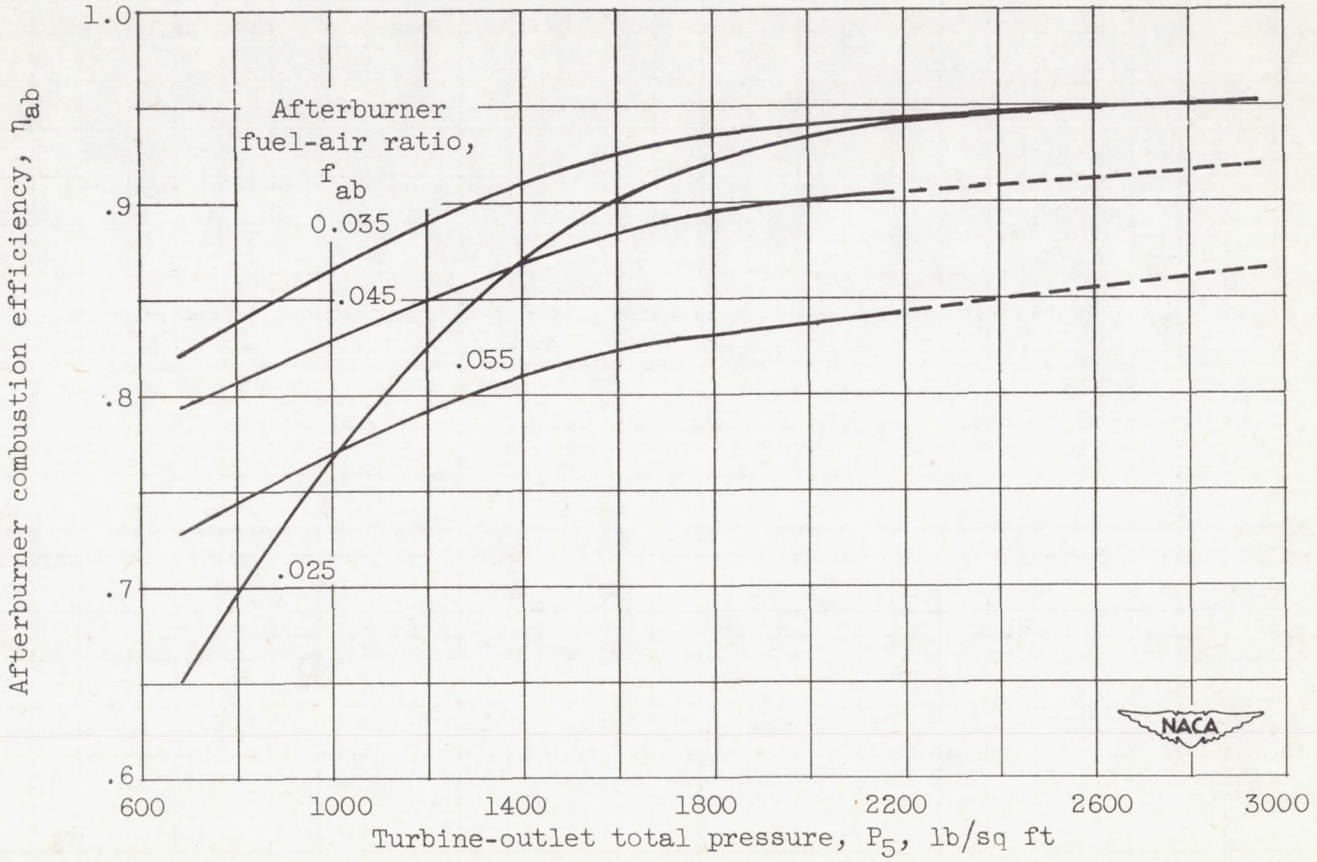

Figure 16. - Effect of turbine-outlet total pressure on combustion efficiency for various afterburner fuel-air ratios for configurations D and E.

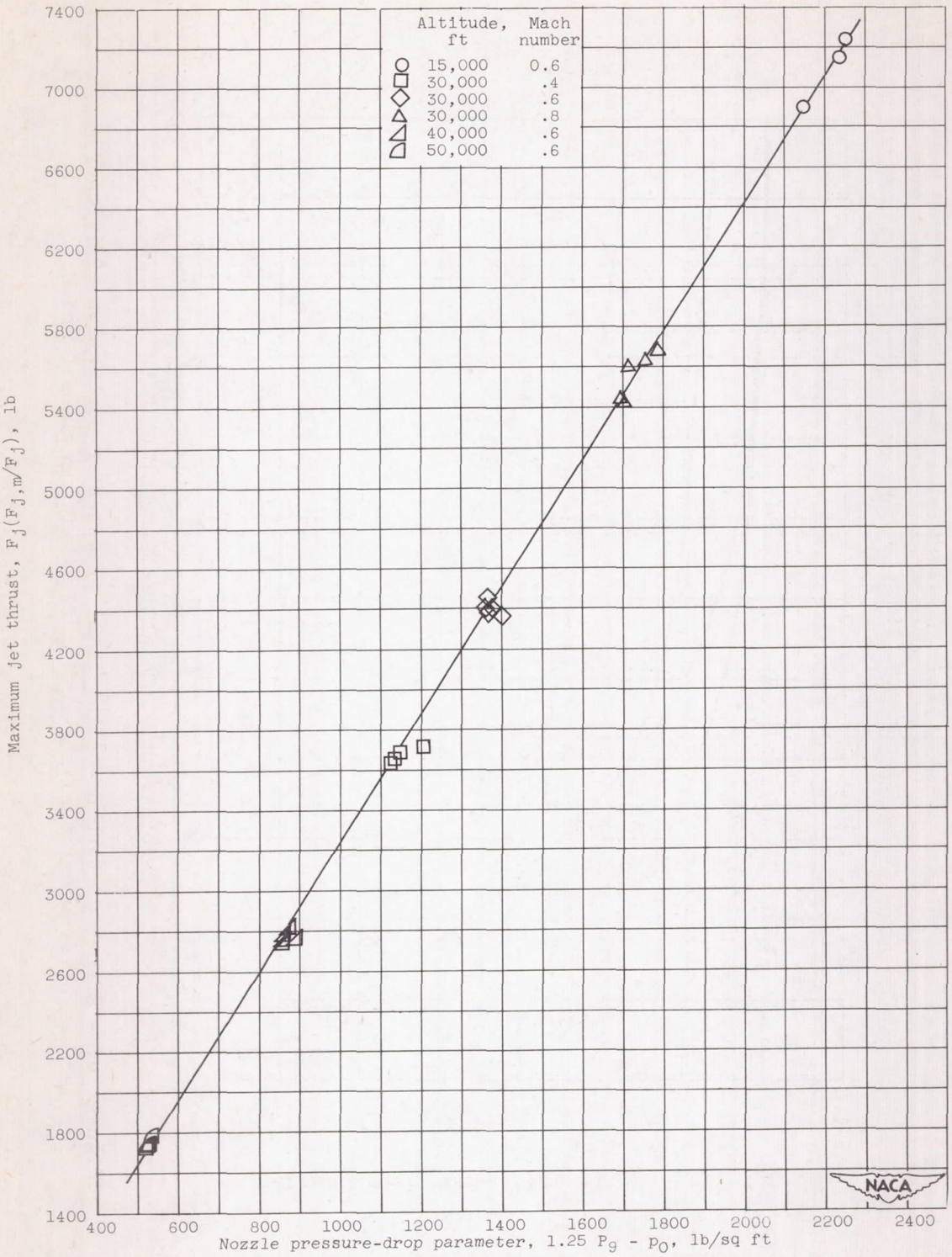

(a) Generalized jet thrust.

Figure 17. - Generalization of afterburning jet thrust for configuration D.

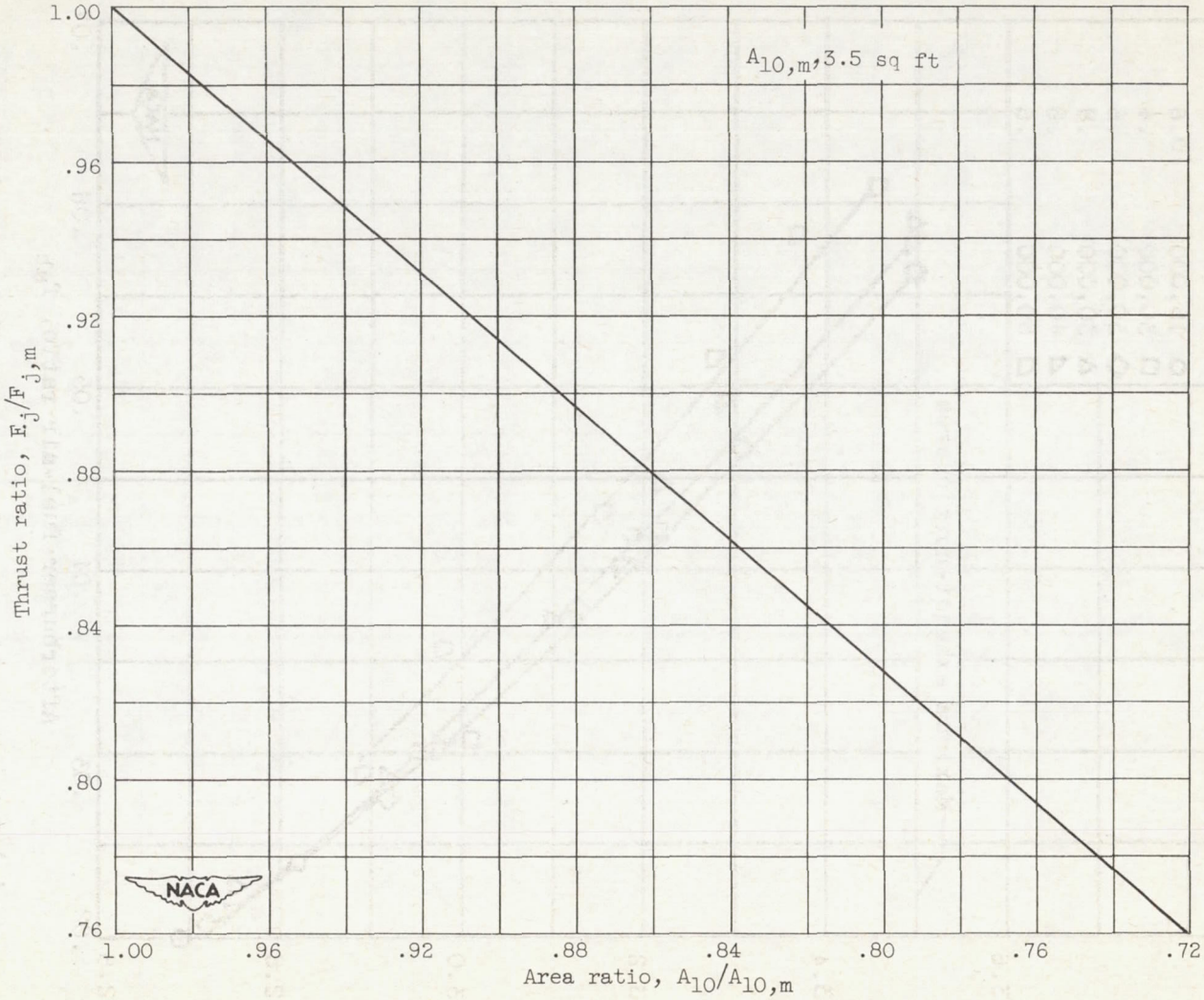

(b) Correction factor for jet thrust obtained from figure 17(a).

Figure 17. - Continued. Generalization of afterburning jet thrust for configuration D.

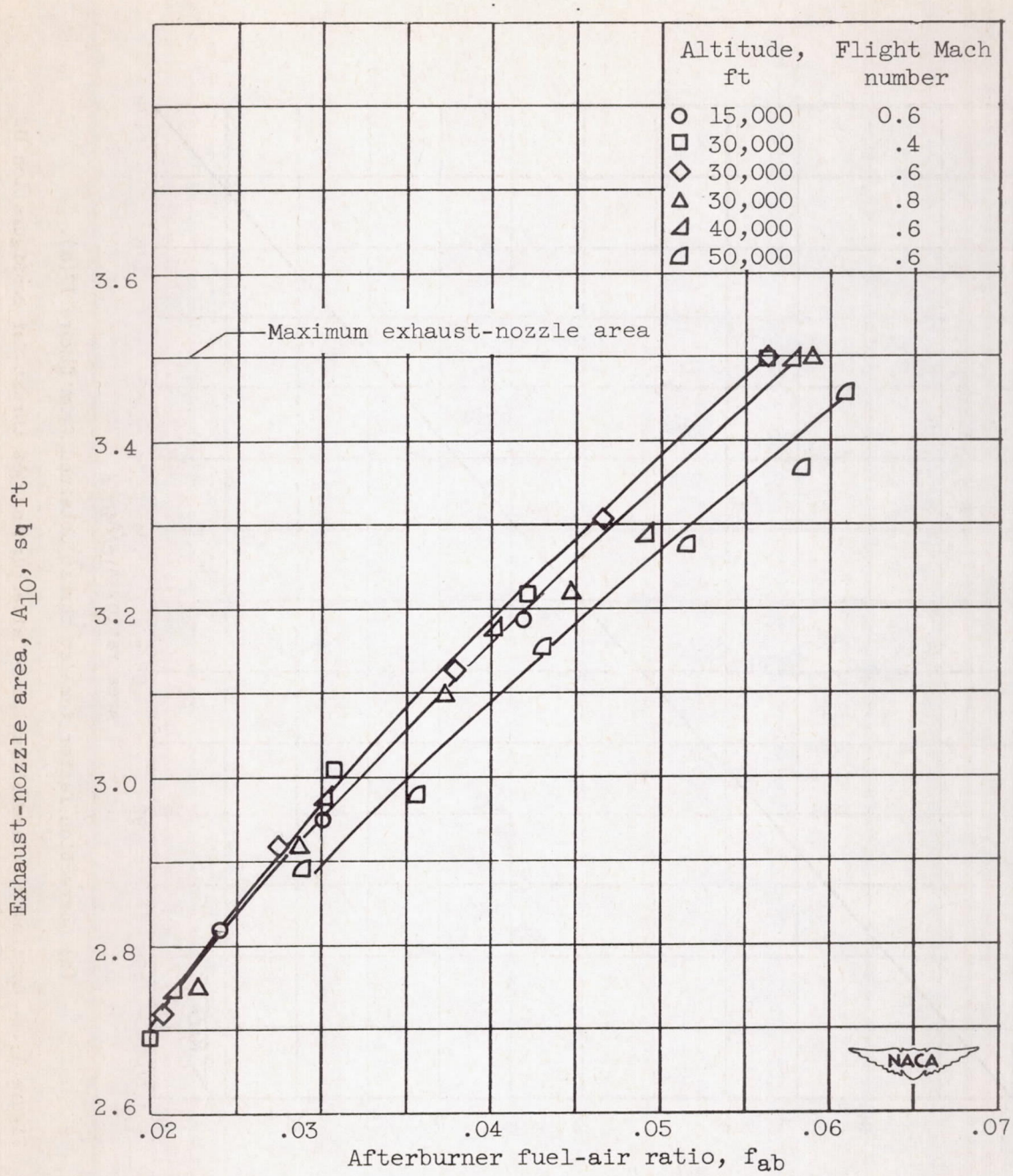

(c) Exhaust-nozzle area for various flight conditions.

Figure 17. - Concluded. Generalization of afterburning jet thrust for configuration D.